Epigenetic Reprogramming of Autophagy Drives Mutant IDH1 Glioma Progression and Response to Radiation

Felipe J Núñez[1,2,†,‡], Kaushik Banerjee[1,2,3,‡], Anzar A. Mujeeb[1,2,3,‡], Ava Mauser[5,‡], Claire E. Tronrud[1,‡], Ziwen Zhu[1,2], Ayman Taher[1,2], Padma Kadiyala[1,2], Stephen V. Carney[1,2,3], Maria B. Garcia-Fabiani[1,2], Andrea Comba[1,2], Mahmoud S. Alghamri[1,2], Brandon L. McClellan[1,2], Syed M. Faisal[1,2], Zeribe C. Nwosu[3,4], Hanna S. Hong[3,4], Tingting Qin[6], Maureen A. Sartor[6], Mats Ljungman[7], Shi-Yuan Cheng[8,9], Henry D. Appelman[10], Pedro R. Lowenstein[1,2,3], Joerg Lahann[5], Costas A. Lyssiotis[3,4,11,*], Maria G. Castro[1,2,3,*].

[1]Department of Neurosurgery, University of Michigan Medical School; Ann Arbor, MI 48109, USA.

[2]Department of Cell and Developmental Biology, University of Michigan Medical School; Ann Arbor, MI 48109, USA.

[3]Rogel Cancer Center, University of Michigan; Ann Arbor, MI 48109, USA

[4]Department of Molecular and Integrative Physiology, University of Michigan; Ann Arbor, MI 48109, USA

[5]Departments of Chemical Engineering, Material Science and Engineering, Biomedical Engineering, and Macromolecular Science and Engineering, University of Michigan; Ann Arbor, MI 48109, USA.

[6]Department of Computational Medicine and Bioinformatics, University of Michigan; Ann Arbor, MI 48109, USA.

[7]Department of Radiation Oncology, University of Michigan; Ann Arbor, MI 48109, USA.

[8]Ken & Ruth Davee Department of Neurology, Northwestern University, Feinberg School of Medicine; Chicago IL 60611, USA.

[9]The Lou and Jean Malnati Brain Tumor Institute, The Robert H. Lurie Comprehensive Cancer Center and Simpson Querrey Institute for Epigenetics, Northwestern University, Feinberg School of Medicine; Chicago IL 60611, USA.

[10]Department of pathology, University of Michigan Medical School; Ann Arbor, MI 48109, USA.

[11]Department of Internal Medicine, Division of Gastroenterology, University of Michigan; Ann Arbor, MI 48109, USA.

*Co-corresponding author: Maria G. Castro, email: mariacas@umich.edu, University of Michigan; 1150 West Medical Center Drive, Ann Arbor, MI 48109-5689

*Co-corresponding author: Costas A. Lyssiotis, Rogel Cancer Center, University of Michigan; Ann Arbor, MI 48109-5942

[†]Current Address: Accenture-Argentina

[‡]Co-First Authors

Abstract

Mutant isocitrate dehydrogenase 1 (mIDH1; IDH1^{R132H}) exhibits a gain of function mutation enabling 2-hydroxyglutarate (2HG) production. 2HG inhibits DNA and histone demethylases, inducing epigenetic reprogramming and corresponding changes to the transcriptome. We previously demonstrated 2HG-mediated epigenetic reprogramming enhances DNA-damage response and confers radioresistance in mIDH1 gliomas harboring p53 and ATRX loss of function mutations. In this study, RNA-seq and ChIP-seq data revealed human and mouse mIDH1 glioma neurospheres have downregulated gene ontologies related to mitochondrial metabolism and upregulated autophagy. Further analysis revealed that the decreased mitochondrial metabolism was paralleled by a decrease in glycolysis, rendering autophagy as a source of energy in mIDH1 glioma cells. Analysis of autophagy pathways showed that mIDH1 glioma cells exhibited increased expression of pULK1-S555 and enhanced LC3 I/II conversion, indicating augmented autophagy activity. This dependence is reflected by increased sensitivity of mIDH1 glioma cells to autophagy inhibition. Blocking autophagy selectively impairs the growth of cultured mIDH1 glioma cells but not wild-type IDH1 (wtIDH1) glioma cells. Targeting autophagy by systemic administration of synthetic protein nanoparticles packaged with siRNA targeting Atg7 (SPNP-siRNA-Atg7) sensitized mIDH1 glioma cells to radiation-induced cell death, resulting in tumor regression, long-term survival, and immunological memory, when used in combination with IR. Our results indicate autophagy as a critical pathway for survival and maintenance of mIDH1 glioma cells, a strategy that has significant potential for future clinical translation.

One Sentence Summary: The inhibition of autophagy sensitizes mIDH1 glioma cells to radiation, thus creating a promising therapeutic strategy for mIDH1 glioma patients.

Introduction

Gliomas are primary brain neoplasms characterized by high morbidity, recurrence, and mortality (*1*). This pathology includes a genetically and phenotypically heterogeneous group of Central Nervous System (CNS) tumors, which are molecularly classified in different subtypes according to the presence of specific genetic lesions and epigenetic profiles (*2, 3*). A gain of function mutation in isocitrate dehydrogenase 1 ($IDH1^{R132H}$; mIDH1) is a common genetic alteration in adult gliomas (*4*). $IDH1^{R132H}$ catalyzes the conversion of α-ketoglutarate to 2-hydroxyglutarate (2HG) (*5*). 2HG inhibits α-ketoglutarate-dependent enzymes such as histone demethylases (KDMs) and cytosine dioxygenases [ten-eleven translocation (TET) methylcytosine dioxygenases], inducing an epigenetic reprogramming of the tumor transcriptome (*6*). $IDH1^{R132H}$ is associated with a better prognosis in gliomas (*4, 7, 8*) and impacts multiple cellular functions, including cell differentiation (*9*), invasion (*10*), immune response (*11-13*), and responses to cellular stress and DNA-damage (*14-16*). We, and others, recently demonstrated that the epigenetic reprogramming in mIDH1 results in enhanced DNA-damage responses and impaired response to radiotherapy (*15-18*). Furthermore, mIDH1 was shown to elicit a cellular metabolic reprogramming that could modify the energetic state of mIDH1 glioma cells and the tumor microenvironment (TME) (*16, 19-22*). The metabolic alterations in mIDH1 gliomas have been associated with a less aggressive tumor phenotype (*16, 23-25*). Mutant IDH1 glioma cells lose the ability to use NADPH-reducing equivalents and gain a novel NADPH-coupled α-ketoglutarate-reducing activity (*26*), resulting in a change in the cellular NADPH to NADP+ ratio (*5*). This leads to enhanced susceptibility to changes in the cellular redox status and oxidative stimuli in mIDH1 glioma cells (*27-30*).

Autophagy is a conserved process that allows the recycling of intracellular components including damaged organelles, protein aggregates and cellular waste, maintaining the energetic homeostasis and protecting cells against stress (*31*). The autophagic pathway involves the

generation and degradation of autophagic vesicles, where the cellular material is collected, contained, processed, and recycled (*32*). This phenomenon occurs in several steps: initiation, expansion, fusion, and degradation, and involves numerous autophagy-related genes (Atg) that participate in an orchestrated assembly, driving the autophagic flux (*33, 34*). This flux can be activated via cell signaling in response to stimulus such as starvation, cellular stress, or DNA-damage (*32, 35, 36*). This physiological process plays crucial roles during development and its deregulation is involved in disease progression, including Parkinson's disease, diabetes, and cancer (*37-41*). The role of autophagy and the mechanisms underlying its regulation in mIDH1 gliomas have not been fully elucidated. For instance, Garry et al., 2014, showed that mutant IDH1/2HG can induce oxidative stress, autophagy, and apoptosis (*14*). In addition, Viswanath et al., 2018, showed that 2HG induces a reduction in the endoplasmic reticulum (ER) via a mechanism termed autophagy of the ER (*42*). They also demonstrated that autophagic flux was higher in both wtIDH1 cells exposed to 2HG and mIDH1 cells (*42*).

In this study, we demonstrate that autophagy plays a critical role in mediating DNA damage response and energetic homeostasis in mouse mIDH1 glioma models and human mIDH1 gliomas co-expressing TP53 and ATRX inactivating mutations (*2, 15*). Through an epigenetic, transcriptomic, metabolomic, and signaling pathway analysis, we show that the epigenetic changes of mIDH1 gliomas, with TP53 and ATRX loss of function mutations, modulate the expression of several genes that functionally impact mitochondrial metabolism and autophagy. We also showed that targeting the autophagy pathway by synthetic protein nanoparticles (SPNPs) incapsulating siRNA against Atg7 enhanced radiosensitivity in mIDH1 mouse glioma model, prolonged survival, and resulted in a sustained immunological memory (*43, 44*). Our findings highlight that autophagy inhibition combined with ionizing radiation (IR) represents an attractive therapeutic strategy that could be implemented for mIDH1 glioma patients.

Results

Transcriptomic reprogramming in mIDH1 glioma impacts autophagy and mitochondrial metabolic pathways

To understand the biological significance of the transcriptomic alteration in mIDH1 glioma, we analyzed the RNA-seq data generated from our previously described mIDH1 mouse glioma model (Fig. 1A) (*15*). We specifically focused on the differential expression of genes related to cellular metabolism and energetic homeostasis. We observed that mIDH1 neurospheres (NS) have upregulated genes related with autophagy gene ontology (Fig. 1B). In addition, these cells have a profound downregulation of electron transport chain (ETC) complex genes (Fig. 1C), suggesting impaired mitochondrial function and bioenergetics. To functionally characterize the differences in metabolic pathways between wtIDH1 and mIDH1, we performed a pathway enrichment analysis. This revealed a downregulation of mitochondrial oxidative-reductive pathways and an enrichment in autophagy (Fig. 1D-F). To determine the effect of mIDH1 on cell metabolism, we performed mass spectrometry-based metabolomics analysis (Fig. S1). We observed that the disrupted mitochondrial respiration gene program (Fig. 1G-H; and Fig. S2-3) is accompanied by the accumulation of tricarboxylic acid (TCA) cycle metabolites (Fig. 1G), suggesting suppressed pathway activity. Consistently, TCA cycle anaplerotic substrates such as aspartate and glutamate (Fig. 1H and Fig. S4), also accumulated in the mIDH1 cells, supporting that mIDH1 disrupts metabolic activities in the glioma NS (Fig. 1I).

Histone hypermethylation in mIDH1 glioma NS is associated with metabolism and autophagy pathways

To evaluate the impact of epigenetic reprogramming mediated by mIDH1 on tumor metabolism and autophagy, we performed ChIP-seq using previously published data generated through native chromatin immunoprecipitation followed by sequencing (Fig. 2A) (*15*). We

evaluated the differential enrichment of H3K4me3, a transcriptional activation mark, and of H3K27me3, a transcriptional repression mark in mIDH1 compared to wtIDH1-NS (Fig. 2B-D). Differential H3K4me3 enriched gene ontology (GO) terms included negative regulation of several cell metabolic processes (Fig. 2B), resulting in an epigenetic downregulation of these metabolic pathways in mIDH1 cells. Similar GO terms were enriched in H3K27me3 histone, indicating an epigenetic repression in mIDH1 glioma NS (Fig. 2C). This was accompanied by enrichment in autophagy pathway in mIDH1 NS (Fig. 2D). Indeed, we observed differential peaks for H3K4me3 around the promoter and genomic regions of the autophagy related gene *Atg9*b in mIDH1 neurospheres (mIDH1-NS) (Fig. 2E). *Atg9b* is a key gene involved in the initial steps of autophagy (*45*, *46*). Consistent with our previous results, our Bru-seq analysis performed on mIDH1-NS showed a higher transcription rate for *Atg9b* (> 2-fold) than wtIDH1-NS (Fig. 2F). Further analysis revealed that mIDH1 cells express higher levels of Atg9b protein in both mouse and human glioma cells (Fig. 2G). These results indicate that mIDH1, through epigenetic reprograming alters metabolic and autophagic pathways in glioma cells (Fig. 2H).

Epigenetic reprogramming in human mIDH1 glioma cells impacts autophagy related genes

In addition to Atg9, the formation of phagophores and autophagosomes requires upregulation of several other genes including *UVRAG*, *STK26* (MST4), *Atg7* and *MAP1LC3B* (Fig. 3A). To further validate the role of mIDH1 in the epigenetic regulation of these genes, we performed a ChIP-seq analysis on SF10602 cells, in the presence or absence of the mIDH1 inhibitor AGI-5198 (Fig. 3B). Our results showed that the specific inhibition of mIDH1 alters peak enrichment for H3K36me3 or H3K4me3 marks (Fig. 3C-G) around genomics regions of *UVRAG* (Fig. 3C), *Atg7* (Fig. 3D), *MAP1LC3B* (Fig. 3E-F) and *STK26* (MST4) (Fig. 3G). This suggests that there is a direct link between IDH1 mutation and upregulation of autophagy related genes in gliomas, in the context of *TP53* and ATRX loss of function.

Single Cell RNA-seq shows an enhancement of autophagy in human mIDH1 glioma cells

To assess the impact of epigenetic reprogramming mediated by mIDH1 on autophagy, scRNA-seq analysis was conducted on SF10602 cells, which harbor the endogenous IDH1-R132H mutation in the context of mutant *ATRX* and *TP53*, under both the presence and absence of the mIDH1 inhibitor AGI-5198 (Fig. 4A). The examination included an evaluation of enriched gene ontology (GO) terms associated with autophagy. The results demonstrated that the inhibition of mIDH1 led to decreased positive regulation of autophagy (Fig. 4B), increased negative regulation of autophagy (Fig. 4C), decreased cellular components of autophagosome (Fig. 4D), and decreased processes utilizing autophagic mechanisms (Fig. 4E). The observed changes in gene ontology terms associated with autophagy highlight a significant influence of mIDH1 on the regulation of autophagy-related processes. The specific alterations identified, such as the modulation of positive and negative regulation of autophagy, as well as changes in cellular components and processes related to autophagosome function, provide valuable insights into the intricate relationship between IDH1 mutation and the dysregulation of autophagy pathways in glioma. Taken together, these findings suggest a link between IDH1 mutation and the upregulation of autophagy-related pathways in glioma.

Mutant IDH1-NS have altered mitochondrial activity and are metabolically quiescent

To gain further insight into the metabolic activity of mIDH1 glioma cells, we used the Seahorse extracellular flux analyzer to compare the bioenergetic profiles of primary NS isolated from wtIDH1 and mIDH1 tumors. Given our transcriptomics analysis indicating dysregulated mitochondrial activity, and the accumulation of the TCA cycle metabolites, we performed the Mito Stress Test to assess differences in mitochondrial function and metabolic profile between wtIDH1 and three different mIDH1-NS clones. When compared to wtIDH1, mIDH1-NS exhibited lower oxygen consumption rate (OCR) at baseline, suggesting mIDH1 glioma cells utilize mitochondrial respiration to a lesser extent compared to that of wtIDH1

cells (Fig. 5A). In line with this finding, the maximal rate of respiration in mIDH1-NS was lower compared to that of wtIDH1 cells, as seen by the reduction in OCR following treatment with the mitochondrial uncoupler 4-(trifluoromethoxy) phenylhydrazone (FCCP) (Fig. 5A and Fig. S5A). Additionally, examination of glycolytic activity, measured by the extracellular acidification rate (ECAR), revealed that mIDH1-NS exhibit a significant reduction (~50%) in ECAR compared to wtIDH1 counterparts at baseline (Fig. 5B and Fig. S5B). Together, these findings demonstrate that mIDH1-NS exhibit less mitochondrial respiration and glycolytic activity, and thus exhibit a quiescent metabolic profile, compared to the wtIDH1-NS (Fig. 5C).

Mutant IDH1 glioma cells promote the conversion of α-ketoglutarate to (R)-2-hydroxyglutarate (2HG), an inhibitor of α-ketoglutarate-dependent epigenetic enzymes. This can modify the transcriptome of tumor cells, and therefore indirectly influence metabolism, in a process that typically requires multiple days and cell divisions (*47*). In contrast, 2HG can also directly impact metabolism by inhibiting metabolic enzymes that use α-ketoglutarate as a substrate, including but not limited to transaminases. In fact, a recent study demonstrated that 2HG can inhibit BCATs, a mechanistic understanding of which identified novel metabolic dependencies in IDH mutant brain tumors (*48*). To determine whether 2HG influences the metabolic profile in our models of mIDH1 tumor cells, wtIDH1-NS were cultured with cell-permeable (R)-2HG (O-2HG) for 4 hours, after which we performed Seahorse extracellular flux analysis. WtIDH1-NS supplemented with O-2HG appeared more similar in basal and maximal respiration to mIDH1 (Fig. 5D), whereas glycolytic activity was impacted to a lesser degree (Fig. 5E). This data illustrates that 2HG supplementation can directly alter the energetic state of glioma NS (Fig. 5F), which likely contributes in part to the observed metabolic changes in mIDH1 cells.

Based on the metabolic defects observed with exogenous 2HG, we then evaluated if mIDH1 glioma cells are more susceptible to mitochondrial inhibitors than those expressing

wtIDH1. To evaluate the sensitivity of mIDH1 to mitochondrial inhibition, we treated wtIDH1-NS or mIDH1-NS with different concentrations of the mitochondrial complex 1 (C1) inhibitors metformin and rotenone (Fig. 5G), after which we evaluated cell viability (Fig. 5H-I and Fig. S6). Results showed that mIDH1-NS were more sensitive to rotenone and metformin treatment than wtIDH1 at later point ($P < 0.001$). Also, inhibition of mitochondrial complex I, renders the mIDH1-mouse NS cells more susceptible to radiation (Fig. S6). There is a significant difference in cell viability when the mIDH1 mouse-NS are treated with either rotenone or metformin in combination with IR compared to radiation alone (Fig. S6).

IDH1 mutation correlates with a fissogenic mitochondrial profile

Mitochondria undergo fusion (elongation) and fission (division) (Fig. 5J), which are critical processes for mitochondrial homeostasis and energy adaptation in response to metabolic changes (*49*). Fusion homogenizes the contents of mitochondria resulting in mitochondrial elongation. Fission consists of mitochondrial fragmentation promoting clearance of damaged mitochondria, closely related with autophagy/mitophagy (*49, 50*). By performing cell labeling, we analyzed the mitochondrial morphology in human and mouse glioma cells expressing wtIDH1, mIDH1 treated with vehicle, or the mIDH1 inhibitor AGI-5198. Wild type IDH1 (wtIDH1-NS) and mIDH1 human glioma cells treated with mIDH1 inhibitor AGI-5198 (SF10602+AGI5198) showed a typical mitochondrial fusion morphology, whereas mIDH1 mouse (mIDH1-NS) and untreated human glioma cells (SF10602) presented a mitochondrial morphology corresponding to fission state (Fig. 5K). These results are consistent with the decreased mitochondrial activity observed in mIDH1 glioma cells, suggesting that mIDH1 glioma cells undergo mitochondrial changes to achieve energetic homeostasis, which can involve the autophagy/mitophagy process.

IDH1-R132H is associated with increased autophagy activation in glioma cells

Our results described above indicate that mIDH1 glioma cells have a disrupted mitochondrial activity with a consequently lower energetic charge when compared with wtIDH1 cells (Fig. 5). This is in line with previous studies indicating that metabolite changes associated with IDH1 mutation alter the energic state of glioma cells (*23, 25, 51*). However, mIDH1 glioma cells can grow and develop tumors in the brains of animals, indicating that they could use alternative mechanisms to generate energy and maintain cell survival. According to our RNA-seq and CHIP-seq data, autophagy is upregulated in mIDH1 glioma cells in correlation with a functional disruption of mitochondrial activity. We then evaluated autophagy activity by protein expression and phosphorylation state of key regulators in the autophagic pathway, including pULK1 (S555) and pULK1 (S757), which are associated with autophagy activation and inhibition, respectively. We also evaluated expression of UVRAG, MST4, and pATG4 that participate in the nucleation and expansion process, involved in autophagome formation in both mIDH1 and wtIDH1 NS (Fig. 6A). Western blot (WB) analysis revealed that in both mouse and human glioma cells, IDH1 mutations results in increased expression of pULK1-(S555) but decreased expression of pULK1-(S757), when compared with wtIDH1 glioma cells (Figs. 6B-C). Moreover, mIDH1 glioma cells showed upregulation of UVRAG, MST4, and pATG4 (*52*) (Figs. 6B-C). Interestingly, inhibition of mIDH1 using AGI-5198 in mIDH1 SF10602 glioma cells reverted the expression pattern of all the key autophagy regulators evaluated (Fig. 6D).

Another important marker of autophagy activation is the conversion of LC3-I to LC3-II (Fig. 6A). A cytosolic form of LC3 (LC3I) is cleaved by Atg4B then conjugated to phosphatidylethanolamine to form LC3-phosphatidylethanolamine conjugate (LC3II), which is recruited to autophagosomal membranes (*53*) during the expansion step of autophagy (Fig. 6A). Thus, the presence and increased intracellular ratio of LC3-II over LC3-I is a signal of autophagy activation. Results showed that in mIDH1 glioma cells, there was more than 4-fold

increase of LC3-II/LC3-I in both human and mouse glioma cells (Figs. 6E-F). As expected, blocking mIDH1 results in 2-fold decrease in the LC3-II/LC3-I ratio (Fig. 6G) These results indicate that IDH1 mutation is associated with autophagy activation in gliomas.

Autophagy flux is enhanced in mIDH1 glioma cells

Autophagy is a continuous process which ends in a recycling of cellular materials (Fig. 6A). During autophagic flux, autophagosomes fuse with lysosomes forming autolysosomes which degrade autophagosome contents (*54*). Using a reporter system where LC3 is fused to both GFP and mCherry (Fig. S7) (*55*), we found that mIDH1 glioma cells had increased number of both autophagosomes and autolysosomes when compared with wt cells (autophagosomes > 10-fold increase, $P < 0.001$; autolysosome > 1.4-fold increase in mIDH1 cells, $P < 0.001$). The increase in autophagosome and autolysosomes could reflect increased autophagy or stalled autophagy. To discern between these two fates, we blocked autophagy with chloroquine (CQ), and we observed an increase in the accumulation of LC3-GFP in mIDH1 glioma cells (autophagosomes > 1.6-fold increase in CQ treated mIDH1 cells, $P < 0.01$; no significance observed in autolysosomes in CQ treated mIDH1 cells vs. CQ treated wt cells) (Fig. 7A-J). In this assay, CQ inhibits autolysosome formation allowing autophagosomes to form and accumulate within the cell. Together, these results indicate that glioma cells harboring IDH1-R132H have an augmented autophagy flux when compared with wtIDH1 glioma cells.

Inhibition of autophagy sensitizes mIDH1 glioma cells to ionizing radiation

Autophagy has been associated with DNA-damage response activation and resistance to ionizing radiation (IR) in tumor cells (*56*). We have previously reported that mIDH1 gliomas are resistant to radiotherapy. We hypothesized that the inhibition of autophagy will impair a proper response against a DNA damage assault in mIDH1 glioma cells, making them more sensitive to IR treatment. To test this hypothesis, we performed a cell viability assay in glioma cells harboring mIDH1, treated with multiple autophagy inhibitors in presence or absence of

irradiation (Fig. 7K-R). We first tested the effect of NSC185058, which targets Atg4b (Fig. 7K) (*52*). Treatment with NSC185058 or irradiation alone decreased IDH1 glioma cells viability compared to vehicle (Fig. 7L-N). However, combination treatment of NSC185058 with IR dramatically decreased mIDH1 glioma cells viability when compared to control or monotherapy (mIDH1 mouse-NS: $P < 0.0001$, Fig. 7L; SJGBM2: $P < 0.001$, Fig. 7M; SF10602: $P < 0.0001$, Fig. 7N). We then tested whether upstream inhibition of the autophagic pathway would be more potent in mIDH1 as a monotherapy. We used ULK101 which inhibits the initial steps of autophagy by targeting ULK1 (Fig. 7O). Monotherapy with ULK101 significantly decreased cell viability in mIDH1 glioma cells (Fig. 7P-R) when compared with control and IR alone ($P < 0.0001$ in all cells). However, combination therapy of IR and ULK101 resulted in a more dramatic decrease in mIDH1 glioma cells viability when compared to control and monotherapy (mIDH1 mouse-NS: $P < 0.05$; SJGBM2: $P < 0.05$; SF10602: $P < 0.001$) or IR alone (mIDH1 mouse-NS: $P < 0.0001$; SJGBM2: $P < 0.001$; SF10602: $P < 0.0001$) (Fig. 7P-R). In addition, we evaluated the impact of the molecular inhibition of autophagy on glioma cells radio-responses through small interfering RNAs (siRNAs; Table S1) against autophagy-related gene ATG7 and ATG4b (Fig. 7S-Z) and through the knockdown of ATG7 in mouse glioma cells (Fig. S8). Using siRNAs (Table S1) against autophagy-related genes ATG7 (Fig. 7S) and ATG4b (Fig. 7W), we assessed the viability of both mouse and human glioma cells treated with radiation. We examined the impact of siRNA-ATG7 (Fig. 7T-V) and siRNA-ATG4b (Fig. 7X-Z) in the presence or absence of IR. Our observations revealed a significant reduction in viability across all tested cells when treated with a combination of siRNAs targeting ATG7 or ATG4b (mIDH1 mouse-NS: $P < 0.0001$; SJGBM2: $P < 0.0001$; SF10602: $P < 0.0001$). In addition, we used a shRNA against ATG7 to generate an autophagy deficient mouse glioma cell (Fig. S13). Like transient autophagy inhibition using siRNA (against ATG7 or ATG4), mIDH1 autophagy deficient cells (mIDH1-ATG7KD) showed

significant radiosensitivity when compared with mIDH1 cells (P < 0.0001) (Fig. S8). The impact of concurrently inhibiting molecular autophagy and applying radiation was assessed in both mouse (Fig. S9) and human glioma cells (Fig. S10) harboring mIDH1. Our observations revealed a notable shift in cytokine profiling, with a significant increase in cytokine concentration observed in mIDH1 glioma cells (Figs S9 and S10; $P < 0.01$) upon combining molecular autophagy inhibition with radiation. These findings suggest the potential of the combined treatment to elicit immune responses in mIDH1 glioma cells. In summary, our results collectively propose that autophagy inhibition not only heightens the sensitivity of mIDH1 glioma cells to radiotherapy but also modulates immune responses.

Molecular inhibition of autophagy prolongs the survival of mIDH1 glioma–bearing mice

To study the impact of autophagy inhibition on mIDH1 tumor *in vivo*, we targeted the autophagy pathway via two approaches: i) a genetically engineered sleeping beauty model that expresses shRNA against Atg7 (shAtg7; Fig. 8A and S13 and S14); and ii) pharmacological inhibition of autophagy pathway using Synthetic protein nanoparticles (SPNPs) loaded with a siRNA targeting Atg7 (Fig. 8A and S11 and S12). The genetically engineered autophagy deficient mouse mIDH1 glioma model was developed using the Sleeping Beauty (SB) Transposon System through a combination of SB-transposase/LUC; NRAS/shP53/GFP; shATRX/GFP; IDH1-R132H/Kat and shAtg7/CFP plasmids (Fig. 8B). We found that mice with *Atg7* KD had a significantly lower median survival (MS) when compared with the control (154 vs. 120 days post-plasmid injection (DPI); $P < 0.001$) (Fig. 8C). We then studied the impact of autophagy inhibition in combination with radiation treatment using our cell implantable mouse mIDH1 glioma model (*15*). We intracranially implanted mIDH1 glioma NS in mice, and 7 days later the animals were split in five groups: i) saline control; ii) treated with empty-SPNPs; iii) treated with IR; iv) treated with SPNPs loaded with small interference RNA against Atg7 (Atg7i-NP); and v) treated with IR + Atg7i-NP at indicated doses and

schedule (Fig. 8D; Table S2). In the genetically engineered mouse mIDH1 glioma model, the autophagy inhibition alone significantly decreased MS ($P < 0.05$) when compared with the control group (Fig. 8D; Table S2). However, IR + Atg7i-NP had a notable impact on MS (MS = 60 DPI; $P < 0.001$) when compared with all the experimental groups (Fig. 8D; Table S2).

Intriguingly, we observed that the combined treatment prolonged the survival of mice long-term (> 90 DPI). Long-term survivors from the IR + Atg7i-NP treatment groups were rechallenged with mIDH1 mouse-NS in the contralateral hemisphere (Fig. 8E). These animals remained tumor free without further treatment, whereas control mice implanted with glioma cells succumbed due to tumor burden (MS = 33 DPI; $P \leq 0.0001$) (Fig. 8E). The animals were sacrificed at 60 DPI after tumor rechallenge, these mice showed no evidence of microscopic intracranial tumor. These results suggest the development of anti-glioma immunological memory in mIDH1 glioma rechallenged animals previously treated with IR + Atg7i-NP. None of these treatments produced hepatic alterations compared with the control group (Figs. S15 and S16).

We then aimed to study the anti–mIDH1 glioma–specific immune response elicited by IR + Atg7i-NP therapy, specifically on T cell proliferation. Mice bearing mIDH1 tumors harboring a surrogate tumor antigen, ovalbumin (OVA), were treated with saline, IR, Atg7i-NP, or IR + Atg7i-NP (Fig. 7F). Mice were euthanized 14 days after the last treatment dose (30 DPI) and the spleen were removed and processed for flow cytometry analysis. Splenocytes were fluorescently labeled with 5- and 6-carboxyfluorescein diacetate succinimidyl ester (CFSE) and stimulated for 4 days with 100 nM SIINFEKL (Fig. 8F), where T cell proliferation was measured as the reduction of CFSE staining in the CD45+/CD3+/CD8+ population. After SIINFEKL treatment, we observed that T cell proliferation was significantly increased ($P < 0.05$) in mIDH1 glioma-bearing mice treated with IR + Atg7i-NP (Fig. 8G and S17) when compared with the control group. This indicates that the combined treatment was able to induce

a systemic anti–mIDH1 glioma–immune response associated with an enhancement in T cell proliferation.

In our investigation, we conducted a comprehensive assessment of tumor growth using histological analysis via H&E staining, along with immunohistochemical markers CD3 (reflecting infiltrating T cells) and CD68 (indicating an inflammatory response or the presence of tumor-associated macrophages) in mice bearing mIDH1 tumors subjected to treatment with ATG7i SPNP + IR. The results revealed a noteworthy reduction in tumor size concomitant with a decrease in the presence of CD3- and CD68-positive cells following the combined treatment, as illustrated in Fig. S18-S19. Taken together, these findings indicate a potent anti-tumor effect, suggesting a multifaceted impact on both T cell infiltration and the inflammatory microenvironment.

Discussion

Metabolic reprogramming is a hallmark alteration observed in glioma patients harboring IDH1^{R132H} mutation (*57*), however the biological consequences and its therapeutic implications remain to be fully elucidated. In this study, we show that in mIDH1 gliomas, in the context of *ATRX* and *TP53* inactivating mutations, autophagy is upregulated in conjunction with functional disruption of mitochondrial activity. Our RNA-seq data displays an upregulation of several autophagy related genes and a downregulation of genes related with mitochondrial metabolism. The downregulation of mitochondrial activity and oxidative phosphorylation is evident in mIDH1 glioma cells, as revealed by the signaling pathway enrichment analysis data. Consistently, mass spectrometry-based metabolomics analysis revealed a marked alteration in the mIDH1 glioma metabolic profile and an alteration of the TCA cycle, with an accumulation of TCA cycle metabolites, suggesting impaired utilization of this pathway. In line with our findings, previous studies suggested that IDH1 mutation modulates TCA cycle, mitochondrial metabolism, and oxidative stress pathways (*16, 20, 23, 58, 59*). The presence of 2HG in glioma cultures reduces both oxidative phosphorylation and ATP levels in glioma cells (*60*). This phenomenon of metabolic alterations is also observed in our genetically engineered mIDH1 glioma model, which shows an upregulation of DNA-damage responses (DDR) (*15*). In addition, the enhancement of DDR has been related with metabolic alterations present in mIDH1 gliomas (*16*). This supports our results showing that the metabolic alterations in mIDH1 glioma cells are involved in the TCA cycle and mitochondrial dysfunctions.

Autophagy is activated in response to mitochondrial dysfunction, serving as a mechanism for cell protection and survival (*61-63*). Our ChIP-seq data confirms that epigenetic reprograming of mIDH1 gliomas impacts the expression of several Atg genes as observed in both mouse and human mIDH1 glioma cells. Our data, obtained by examination of OCR and

ECAR, revealed that mitochondrial and glycolytic activity are reduced in mIDH1 glioma cells. These results functionally support our molecular data, indicating a mitochondrial dysfunction along with an energetic state as encountered in quiescent cells. It has been suggested that autophagy may provide nutrients necessary to meet bioenergetic demands during transition from quiescence to energy dependent cell states (*64*). Furthermore, it has been demonstrated that mitophagy, the mitochondrial autophagy, can be induced by redox mitochondrial agents in cancer cells (*62*). Our results demonstrate that human and mouse mIDH1 glioma cells present morphological characteristics indicative of the mitochondrial fission process, which is tightly related with autophagy/mitophagy (*49*). Using an autophagy flux assay and WB to detect activation of *ATG* genes, the conversion of LC3-I to LC3-II, which is one of the distinctive hallmarks of autophagy (*65*), we demonstrated that autophagy activity is functionally increased in mouse and human mIDH1 glioma cells. We show that the inhibition of $IDH1^{R132H}$ reverts this phenotype in patient-derived mIDH1 glioma cells, suggesting that the enhancement of autophagy is 2HG dependent. Our study describes epigenetic mechanisms involved in this phenotype, where histone methylation plays a key role in metabolic reprogramming and activation of autophagy.

According to our results, autophagy could serve as a cell protection and survival mechanism in mIDH1 gliomas. It has been described that autophagy has an impact on cancer therapeutic responses (*66-71*). We evaluated the impact of autophagy inhibition in response to radiation *in vitro* and *in vivo*. Our results indicate that autophagy inhibition sensitizes mIDH1 glioma cells to IR treatment, decreasing cell viability of mouse glioma NS and human glioma cells. This is supported by the fact that autophagy can induce DNA-damage response activation, thus inducing resistance to IR in tumor cells (*56*). We generated a genetically engineered autophagy deficient mIDH1 mouse glioma model, which displayed a decreased median survival when compared with the control mIDH1 glioma mouse model. These results

are consistent with known roles autophagy has played in contributing to a tumorigenic environment, such as the protective role of autophagy in the presence of DNA damage (*36*) and its role in maintaining chromosomal stability (*72-74*). Our results show an upregulation of *UVRAG*, an Atg gene involved in chromosomal stability, which is in line with an increased DDR reported in mIDH1 gliomas (*15, 16*). Conversely, this phenomenon could increase cell protection against DNA damage assault and contribute to radio-resistance. Using our cell implantable mIDH1 glioma model (*15*), we evaluated the therapeutic impact of autophagy inhibition using SPNPs loaded with siRNA targeting Atg7 (Atg7i-SPNP) in combination with IR. This combination increased median survival and elicited 40% of long-term tumor-free survivors in mIDH1 glioma bearing mice, demonstrating that autophagy inhibition sensitizes mIDH1 tumors to radiotherapy. In addition, our re-challenge experiment displayed a 100% survival rate of mIDH1 animals that were previously treated with IR in combination with Atg7i-SPNP. These results also indicated that the combined therapeutic approach induces anti-tumor immunological memory (*22*). This was confirmed when we observed increased tumor-antigen specific T cell proliferation in mIDH1 glioma animals treated with IR and Atg7i-SPNP.

Our work demonstrates that autophagy activation leads to radioresistance in patient-derived mIDH1 low grade glioma (LGG) cell cultures. Furthermore, we show that when radiation was delivered in combination with autophagy inhibition (ATG7i-SPNP), the mIDH1 gliomas become radiosensitive which leads to long-term survival and anti-tumor immunological memory (Fig. 8). However, evaluating these responses in patient-derived glioma models is limited because patient-derived cells failed to form tumors in immunodeficient mice. Our past experiences with genetically engineered animal models, which recapitulate critical features observed in glioma patients and molecular databases (*12, 15, 22, 75*), gave us confidence that our results are relevant to a better understanding of the biological significance of metabolic reprograming observed in mIDH1 gliomas and the

involvement of autophagy in mediating therapeutic responses. Our results also apply to a particular mIDH1 molecular subtype, which harbors concomitant inactivating mutations in TP53 and ATRX, recently classified by the World Health Organization as astrocytomas. This genotype was included in all *in vitro*, *ex vivo*, and *in vivo* experiments presented.

The molecular, functional, and pre-clinical data of mIDH1 gliomas indicate that the epigenetic reprograming on mitochondrial metabolic activity, which is downregulated when autophagy is enhanced, influences therapeutic responses. Through this study, we have shown that inhibiting autophagy not only radiosensitizes *in vivo* mIDH1 glioma tumors, but also leads to increased survival and anti-tumor immunological memory (Fig. 8); thus, providing a promising and novel therapeutic combination treatment that could be further developed and implemented in mIDH1 glioma patients.

Study Design

To study the impact of autophagy in the context of IDH1^{R132H} mutant gliomas, with *TP53* and *ATRX* inactivating mutations, we previously generated a genetically engineered animal model injecting SB plasmids encoding NRAS G12V, shp53, with or without shATRX, and with or without IDH1^{R132H} into the lateral ventricle of neonatal mice (*15*). Sample size and any data inclusion/exclusion were defined individually for each experiment. We also used an animal model previously generated by intracranial implantation of glioma NS (wt-IDH1 and mIDH1) derived from our genetically engineered animal model to test therapeutic responses (*15*). Furthermore, we used human glioma cells derived from patients harboring IDH1^{R132H}, in the context of *TP53* and *ATRX* inactivating mutations, to confirm the results obtained from our animal models. The number of replicates are reported in the figure legends. Our studies were not randomized. We performed blinding for quantitative IHC scoring. All RNA-seq and ChIP-seq data were deposited in public databases as is indicated in the respective sections. Materials and Methods are detailed in the Supplementary Materials.

Genetically engineered mutant IDH1 glioma model

All animal studies were conducted according to guidelines approved by the Institutional Animal Care and Use Committee at the University of Michigan. All animals were housed in an AAALAC accredited animal facility; and they were monitored daily. Studies did not discriminate sex, and both male and females were used. The strains of mice used in the study were C57BL/6 (The Jackson Laboratories, 000664).

The wild type (wt)-IDH1 and mIDH1 glioma models used in this study were generated previously for our group using SB Transposon System (1). The plasmid used to generate those models are: (i) SB transposase and luciferase (pT2C-LucPGK-SB100X, henceforth referred to as SB/Luc), (ii) a constitutively active mutant of NRAS, NRAS-G12V (pT2CAG-NRASV12, henceforth referred to as NRAS), (iii) a short hairpin against p53 (pT2-shp53-GFP4, henceforth

referred to as shp53), (iv) a short hairpin against ATRX (pT2-shATRX53-GFP4, henceforth referred to as shATRX), and (v) mutant IDH1^{R132H} (pKT-IDH1(R132H)-IRES-Katushka, henceforth referred to as mIDH1). Neonatal P01 wt C57BL/6 mice were used in all experiments. The genotype of SB- generated mice involved these combinations: (i) NRAS, shP53, and shATRX (wtIDH1) and (ii) NRAS, shp53, shATRX, and IDH1^{R132H} (mIDH1). Mice were injected according to a previously described protocol (2). Plasmids were mixed in mass ratios of 1:2:2:2 or 1:2:2:2:2 (20 µg plasmid in a total of 40 µL plasmid mixture) with in vivo-jetPEI (Polyplus Transfection, 201-50G) (2.8 µL per 40 µL plasmid mixture) and dextrose (5% total) and maintained at room temperature for at least 15 min prior to injection. The lateral ventricle (1.5 mm AP, 0.7 mm lateral, and 1.5 mm deep from lambda) of neonatal mice (P01) was injected with 0.75 µL plasmid mixture (0.5 µL/min) that included: (1) SB/Luc, (2) NRAS, (3) shp53, (4) with or without shATRX, and (5) with or without IDH1^{R132H}. To monitor plasmid uptake in neonatal pups, 30 µL of luciferin (30 mg/mL) was injected subcutaneously into each pup 24-48 hours after plasmid injection. In vivo bioluminescence was measured on an IVIS Spectrum (Perkin Elmer, 124262) imaging system. For the IVIS spectrum, the following settings were used: automatic exposure, large binning, and aperture f = 1. Pups without luminescence were euthanized according to an approved protocol: Committee on Use and Care of Animals (UCUCA) PRO00007617. For *in vivo* imaging of tumor formation and progression in adult mice, 100 µL of luciferin solution was injected intra-peritoneally (ip) and mice were then anesthetized with oxygen/isoflurane (1.5-2.5% isoflurane). To score luminescence, Living Image Software Version 4.3.1 (Caliper Life Sciences) was used. A region of interest (ROI) was defined as a circle over the head, and luminescence intensity was measured using the calibrated unit's photons/s/cm2/sr. Multiple images were taken over a 25-minute period following injection, and maximal intensity was reported.

For survival studies, animals were monitored daily for signs of morbidity, including ataxia, impaired mobility, hunched posture, seizures, and scruffy fur. Animals displaying symptoms of morbidity were intracardially perfused using Tyrode's solution, followed by fixation with 4% paraformaldehyde (PFA) in phosphate buffered saline (PBS).

Generation of iRGD Synthetic Protein Nanoparticle (SPNP) with siRNA against *Atg7*

The Atg7 Mouse siRNA Oligo Duplex (Locus ID 74244) (Origene, SR427399) was used to generate iRGD SPNP.

SPNP formulation:

The preparation of the SPNP formulations followed previously reported methods but with modifications (10). In the basic formulation, two solutions were prepared separately then combined. Human serum albumin (7.5% w/v) was solubilized in a solvent system comprised of ultrapure deionized water and ethylene glycol (80:20 v/v). The peptide, iRGD was then added along with BSA Alexa Fluor 647 conjugate (0.25% w/w relative to the albumin) to produce fluorescently labeled SPNPs. Then, the siRNA, which was resuspended according to the manufacturer's protocol, was complexed for 30 minutes at room temperature under rotation with 60 kDa branched polyethyleneimine (5% w/v) before also being added to the serum albumin solution. Next, a bi-functional macromer, O,O'-Bis[2-N-Succinimidyl-succinylamino)ethyl]polyethylene glycol, was added at 10% w/w relative to the human serum albumin solution. Once mixed, the two solutions were mixed to form the final formulation. For empty SPNP groups, all the components that were added in the iRGD ATG7 siRNA SPNPs were included except for the ATG7 siRNA.

SPNP fabrication

SPNPs were fabricated via electrohydrodynamic jetting (10). The parameters used were the same as previously described. Briefly, the final formulation was loaded into 1 mL syringes equipped with a 1.5" 25-gauge stainless steel blunt needle. It was pumped at a rate of 0.2

mL/hour to form droplets at the base of the needle. A voltage source was connected to the needle and grounded at the collection plate, located 6 inches from the base of the pump. The voltage was adjusted typically to a range between 8 kV and 15 kV to achieve a stable Taylor cone whereby rapid evaporation of the solvent occurred, creating solid nanoparticles on the collection plate. The collection plate was replaced with a clean plate every 30 minutes until the solution within the syringe emptied. The collection plates were enclosed and incubated for 7 days at 37˚C to form stable crosslinks.

SPNP collection and processing

After the one-week period of incubation, the SPNPs on collection plates were removed. About 3-4mL of 0.01% Tween 20 in DPBS was added to each pan and physically agitated with plastic razor blades to release the SPNPs off the plate. The SPNP suspension was collected into a falcon tube. Each pan was agitated with fresh 0.01% Tween 20 in DPBS three times. The collected SPNPs was tip sonicated at an amplitude of 7 for 30 seconds (1 second on and 3 seconds off) in an ice bath to break up aggregates, strained through a 40 µm filter into a new falcon tube then centrifuged at 3220 RCF for 5 minutes. The supernatant was removed and distributed into 2 mL Eppendorf tubes and centrifuged for 1 hour at 4˚C at 21,500 RCF. The supernatant was discarded, and the resulting pellets were combined into a single 2 mL tube. The particles were washed two times with fresh DPBS without Tween 20.

SPNP characterization

Scanning electron Microscopy (SEM): SEM samples were prepared by placing a silicon wafer on top of the collection plate during the jetting process. The samples were then placed on a copper tape covered SEM stub, then gold coated for 40 seconds and visualized through the FEI NOVA 200 SEM/FIB instrument. The dry state SPNP quantification of morphology parameters were conducted through ImageJ analysis as described previously (11).

Dynamic Light Scattering (DLS): The hydrodynamic diameter and zeta potential was determined through DLS on the Malvern Zetasizer. Samples were prepared by diluting the stock sample in DPBS and measured in folded capillary zeta cells. An average of at least three measurements was used to characterize each sample.

Bicinchoninic acid assay (BCA assay): BCA assay was used to quantify SPNP concentration. A standard curve was prepared for every SPNP concentration quantification measurement.

Statistical analysis

All quantitative data are presented as the means ± SEM from at least three independent samples. ANOVA and two-sample *t* tests were used to compare continuous outcomes between groups. Survival curves were analyzed using the Kaplan-Meier method and compared using Mantel-Cox tests; the effect size is expressed as median survival (MS). Differences were considered significant if $P < 0.05$. All analyses were conducted using GraphPad Prism software (version 6.01), SAS (version 9.4, SAS Institute), or R (version 3.1.3). The statistical tests used are indicated in each figure legend.

References

1. M. Weller, W. Wick, K. Aldape, M. Brada, M. Berger, S. M. Pfister, R. Nishikawa, M. Rosenthal, P. Y. Wen, R. Stupp, G. Reifenberger, Glioma. *Nature Reviews Disease Primers* **1**, 15017 (2015).
2. M. Ceccarelli, Floris P. Barthel, Tathiane M. Malta, Thais S. Sabedot, Sofie R. Salama, Bradley A. Murray, O. Morozova, Y. Newton, A. Radenbaugh, Stefano M. Pagnotta, S. Anjum, J. Wang, G. Manyam, P. Zoppoli, S. Ling, Arjun A. Rao, M. Grifford, Andrew D. Cherniack, H. Zhang, L. Poisson, Carlos G. Carlotti, Daniela Pretti da C. Tirapelli, A. Rao, T. Mikkelsen, Ching C. Lau, W. K. A. Yung, R. Rabadan, J. Huse, Daniel J. Brat, Norman L. Lehman, Jill S. Barnholtz-Sloan, S. Zheng, K. Hess, G. Rao, M. Meyerson, R. Beroukhim, L. Cooper, R. Akbani, M. Wrensch, D. Haussler, Kenneth D. Aldape, Peter W. Laird, David H. Gutmann, S. Anjum, H. Arachchi, J. T. Auman, M. Balasundaram, S. Balu, G. Barnett, S. Baylin, S. Bell, C. Benz, N. Bir, Keith L. Black, T. Bodenheimer, L. Boice, Moiz S. Bootwalla, J. Bowen, Christopher A. Bristow, Yaron S. N. Butterfield, Q.-R. Chen, L. Chin, J. Cho, E. Chuah, S. Chudamani, Simon G. Coetzee, Mark L. Cohen, H. Colman, M. Couce, F. D'Angelo, T. Davidsen, A. Davis, John A. Demchok, K. Devine, L. Ding, R. Duell, J. B. Elder, Jennifer M. Eschbacher, A. Fehrenbach, M. Ferguson, S. Frazer, G. Fuller, J. Fulop, Stacey B. Gabriel, L. Garofano, Julie M. Gastier-Foster, N. Gehlenborg, M. Gerken, G. Getz, C. Giannini, William J. Gibson, A. Hadjipanayis, D. N. Hayes, David I. Heiman, B. Hermes, J. Hilty, Katherine A. Hoadley, Alan P. Hoyle, M. Huang, Stuart R. Jefferys, Corbin D. Jones, Steven J. M. Jones, Z. Ju, A. Kastl, A. Kendler, J. Kim, R. Kucherlapati, Phillip H. Lai, Michael S. Lawrence, S. Lee, Kristen M. Leraas, Tara M. Lichtenberg, P. Lin, Y. Liu, J. Liu, Julia Y. Ljubimova, Y. Lu, Y. Ma, Dennis T. Maglinte, Harshad S. Mahadeshwar, Marco A. Marra, M. McGraw, C. McPherson, S. Meng, Piotr A. Mieczkowski, C. R. Miller, Gordon B. Mills, Richard A. Moore, Lisle E. Mose, Andrew J. Mungall, R. Naresh, T. Naska, L. Neder, Michael S. Noble, A. Noss, Brian P. O'Neill, Quinn T. Ostrom, C. Palmer, A. Pantazi, M. Parfenov, Peter J. Park, Joel S. Parker, Charles M. Perou, Christopher R. Pierson, T. Pihl, A. Protopopov, A. Radenbaugh, Nilsa C. Ramirez, W. K. Rathmell, X. Ren, J. Roach, A. G. Robertson, G. Saksena, Jacqueline E. Schein, Steven E. Schumacher, J. Seidman, K. Senecal, S. Seth, H. Shen, Y. Shi, J. Shih, K. Shimmel, H. Sicotte, S. Sifri, T. Silva, Janae V. Simons, R. Singh, T. Skelly, Andrew E. Sloan, Heidi J. Sofia, Matthew G. Soloway, X. Song, C. Sougnez, C. Souza, Susan M. Staugaitis, H. Sun, C. Sun, D. Tan, J. Tang, Y. Tang, L. Thorne, Felipe A. Trevisan, T. Triche, David J. Van Den Berg, U. Veluvolu, D. Voet, Y. Wan, Z. Wang, R. Warnick, John N. Weinstein, Daniel J. Weisenberger, Matthew D. Wilkerson, F. Williams, L. Wise, Y. Wolinsky, J. Wu, Andrew W. Xu, L. Yang, L. Yang, Travis I. Zack, Jean C. Zenklusen, J. Zhang, W. Zhang, J. Zhang, E. Zmuda, H. Noushmehr, A. Iavarone, R. G. W. Verhaak, Molecular Profiling Reveals Biologically Discrete Subsets and Pathways of Progression in Diffuse Glioma. *Cell* **164**, 550-563 (2016).
3. D. N. Louis, A. Perry, G. Reifenberger, A. von Deimling, D. Figarella-Branger, W. K. Cavenee, H. Ohgaki, O. D. Wiestler, P. Kleihues, D. W. Ellison, The 2016 World Health Organization Classification of Tumors of the Central Nervous System: a summary. *Acta Neuropathologica* **131**, 803-820 (2016).
4. D. J. Brat, R. G. Verhaak, K. D. Aldape, W. K. Yung, S. R. Salama, L. A. Cooper, E. Rheinbay, C. R. Miller, M. Vitucci, O. Morozova, A. G. Robertson, H. Noushmehr, P. W. Laird, A. D. Cherniack, R. Akbani, J. T. Huse, G. Ciriello, L. M. Poisson, J. S. Barnholtz-Sloan, M. S. Berger, C. Brennan, R. R. Colen, H. Colman, A. E. Flanders, C. Giannini, M. Grifford, A. Iavarone, R. Jain, I. Joseph, J. Kim, K. Kasaian, T. Mikkelsen, B. A. Murray, B. P. O'Neill, L. Pachter, D. W. Parsons, C. Sougnez, E. P. Sulman, S. R. Vandenberg, E. G. Van Meir, A. von Deimling, H. Zhang, D. Crain, K. Lau, D. Mallery, S. Morris, J. Paulauskis, R. Penny, T. Shelton, M. Sherman, P. Yena, A. Black, J. Bowen, K. Dicostanzo, J. Gastier-Foster, K. M. Leraas, T. M. Lichtenberg, C. R. Pierson, N. C. Ramirez, C. Taylor, S. Weaver, L. Wise, E. Zmuda, T. Davidsen, J. A.

Demchok, G. Eley, M. L. Ferguson, C. M. Hutter, K. R. Mills Shaw, B. A. Ozenberger, M. Sheth, H. J. Sofia, R. Tarnuzzer, Z. Wang, L. Yang, J. C. Zenklusen, B. Ayala, J. Baboud, S. Chudamani, M. A. Jensen, J. Liu, T. Pihl, R. Raman, Y. Wan, Y. Wu, A. Ally, J. T. Auman, M. Balasundaram, S. Balu, S. B. Baylin, R. Beroukhim, M. S. Bootwalla, R. Bowlby, C. A. Bristow, D. Brooks, Y. Butterfield, R. Carlsen, S. Carter, L. Chin, A. Chu, E. Chuah, K. Cibulskis, A. Clarke, S. G. Coetzee, N. Dhalla, T. Fennell, S. Fisher, S. Gabriel, G. Getz, R. Gibbs, R. Guin, A. Hadjipanayis, D. N. Hayes, T. Hinoue, K. Hoadley, R. A. Holt, A. P. Hoyle, S. R. Jefferys, S. Jones, C. D. Jones, R. Kucherlapati, P. H. Lai, E. Lander, S. Lee, L. Lichtenstein, Y. Ma, D. T. Maglinte, H. S. Mahadeshwar, M. A. Marra, M. Mayo, S. Meng, M. L. Meyerson, P. A. Mieczkowski, R. A. Moore, L. E. Mose, A. J. Mungall, A. Pantazi, M. Parfenov, P. J. Park, J. S. Parker, C. M. Perou, A. Protopopov, X. Ren, J. Roach, T. S. Sabedot, J. Schein, S. E. Schumacher, J. G. Seidman, S. Seth, H. Shen, J. V. Simons, P. Sipahimalani, M. G. Soloway, X. Song, H. Sun, B. Tabak, A. Tam, D. Tan, J. Tang, N. Thiessen, T. Triche, Jr., D. J. Van Den Berg, U. Veluvolu, S. Waring, D. J. Weisenberger, M. D. Wilkerson, T. Wong, J. Wu, L. Xi, A. W. Xu, L. Yang, T. I. Zack, J. Zhang, B. A. Aksoy, H. Arachchi, C. Benz, B. Bernard, D. Carlin, J. Cho, D. DiCara, S. Frazer, G. N. Fuller, J. Gao, N. Gehlenborg, D. Haussler, D. I. Heiman, L. Iype, A. Jacobsen, Z. Ju, S. Katzman, H. Kim, T. Knijnenburg, R. B. Kreisberg, M. S. Lawrence, W. Lee, K. Leinonen, P. Lin, S. Ling, W. Liu, Y. Liu, Y. Liu, Y. Lu, G. Mills, S. Ng, M. S. Noble, E. Paull, A. Rao, S. Reynolds, G. Saksena, Z. Sanborn, C. Sander, N. Schultz, Y. Senbabaoglu, R. Shen, I. Shmulevich, R. Sinha, J. Stuart, S. O. Sumer, Y. Sun, N. Tasman, B. S. Taylor, D. Voet, N. Weinhold, J. N. Weinstein, D. Yang, K. Yoshihara, S. Zheng, W. Zhang, L. Zou, T. Abel, S. Sadeghi, M. L. Cohen, J. Eschbacher, E. M. Hattab, A. Raghunathan, M. J. Schniederjan, D. Aziz, G. Barnett, W. Barrett, D. D. Bigner, L. Boice, C. Brewer, C. Calatozzolo, B. Campos, C. G. Carlotti, Jr., T. A. Chan, L. Cuppini, E. Curley, S. Cuzzubbo, K. Devine, F. DiMeco, R. Duell, J. B. Elder, A. Fehrenbach, G. Finocchiaro, W. Friedman, J. Fulop, J. Gardner, B. Hermes, C. Herold-Mende, C. Jungk, A. Kendler, N. L. Lehman, E. Lipp, O. Liu, R. Mandt, M. McGraw, R. McLendon, C. McPherson, L. Neder, P. Nguyen, A. Noss, R. Nunziata, Q. T. Ostrom, C. Palmer, A. Perin, B. Pollo, A. Potapov, O. Potapova, W. K. Rathmell, D. Rotin, L. Scarpace, C. Schilero, K. Senecal, K. Shimmel, V. Shurkhay, S. Sifri, R. Singh, A. E. Sloan, K. Smolenski, S. M. Staugaitis, R. Steele, L. Thorne, D. P. Tirapelli, A. Unterberg, M. Vallurupalli, Y. Wang, R. Warnick, F. Williams, Y. Wolinsky, S. Bell, M. Rosenberg, C. Stewart, F. Huang, J. L. Grimsby, A. J. Radenbaugh, J. Zhang, Comprehensive, Integrative Genomic Analysis of Diffuse Lower-Grade Gliomas. *N Engl J Med* **372**, 2481-2498 (2015).

5. L. Dang, D. W. White, S. Gross, B. D. Bennett, M. A. Bittinger, E. M. Driggers, V. R. Fantin, H. G. Jang, S. Jin, M. C. Keenan, K. M. Marks, R. M. Prins, P. S. Ward, K. E. Yen, L. M. Liau, J. D. Rabinowitz, L. C. Cantley, C. B. Thompson, M. G. Vander Heiden, S. M. Su, Cancer-associated IDH1 mutations produce 2-hydroxyglutarate. *Nature* **462**, 739-744 (2009).
6. J.-A. Losman, P. Koivunen, W. G. Kaelin, 2-Oxoglutarate-dependent dioxygenases in cancer. *Nature Reviews Cancer* **20**, 710-726 (2020).
7. Comprehensive, Integrative Genomic Analysis of Diffuse Lower-Grade Gliomas. *New England Journal of Medicine* **372**, 2481-2498 (2015).
8. D. W. Parsons, S. Jones, X. Zhang, C.-H. Lin Jimmy, J. Leary Rebecca, P. Angenendt, P. Mankoo, H. Carter, I. M. Siu, L. Gallia Gary, A. Olivi, R. McLendon, B. A. Rasheed, S. Keir, T. Nikolskaya, Y. Nikolsky, A. Busam Dana, H. Tekleab, A. Diaz Luis, J. Hartigan, R. Smith Doug, L. Strausberg Robert, N. Marie Suely Kazue, O. Shinjo Sueli Mieko, H. Yan, J. Riggins Gregory, D. Bigner Darell, R. Karchin, N. Papadopoulos, G. Parmigiani, B. Vogelstein, E. Velculescu Victor, W. Kinzler Kenneth, An Integrated Genomic Analysis of Human Glioblastoma Multiforme. *Science* **321**, 1807-1812 (2008).
9. D. Rohle, J. Popovici-Muller, N. Palaskas, S. Turcan, C. Grommes, C. Campos, J. Tsoi, O. Clark, B. Oldrini, E. Komisopoulou, K. Kunii, A. Pedraza, S. Schalm, L. Silverman, A. Miller, F. Wang, H. Yang, Y. Chen, A. Kernytsky, K. Rosenblum Marc, W. Liu, A. Biller Scott, M. Su Shinsan, W.

Brennan Cameron, A. Chan Timothy, G. Graeber Thomas, E. Yen Katharine, K. Mellinghoff Ingo, An Inhibitor of Mutant IDH1 Delays Growth and Promotes Differentiation of Glioma Cells. *Science* **340**, 626-630 (2013).

10. A. L. Baldock, K. Yagle, D. E. Born, S. Ahn, A. D. Trister, M. Neal, S. K. Johnston, C. A. Bridge, D. Basanta, J. Scott, H. Malone, A. M. Sonabend, P. Canoll, M. M. Mrugala, J. K. Rockhill, R. C. Rockne, K. R. Swanson, Invasion and proliferation kinetics in enhancing gliomas predict IDH1 mutation status. *Neuro-Oncology* **16**, 779-786 (2014).

11. N. M. Amankulor, Y. Kim, S. Arora, J. Kargl, F. Szulzewsky, M. Hanke, D. H. Margineantu, A. Rao, H. Bolouri, J. Delrow, D. Hockenbery, A. M. Houghton, E. C. Holland, Mutant IDH1 regulates the tumor-associated immune system in gliomas. *Genes Dev* **31**, 774-786 (2017).

12. S. Alghamri Mahmoud, L. McClellan Brandon, P. Avvari Ruthvik, R. Thalla, S. Carney, S. Hartlage Carson, S. Haase, M. Ventosa, A. Taher, N. Kamran, L. Zhang, M. Faisal Syed, J. Núñez Felipe, B. Garcia-Fabiani María, N. Al-Holou Wajd, D. Orringer, S. Hervey-Jumper, J. Heth, G. Patil Parag, K. Eddy, D. Merajver Sofia, J. Ulintz Peter, J. Welch, C. Gao, J. Liu, G. Núñez, D. Hambardzumyan, R. Lowenstein Pedro, G. Castro Maria, G-CSF secreted by mutant IDH1 glioma stem cells abolishes myeloid cell immunosuppression and enhances the efficacy of immunotherapy. *Science Advances* **7**, eabh3243.

13. M. Platten, L. Bunse, A. Wick, T. Bunse, L. Le Cornet, I. Harting, F. Sahm, K. Sanghvi, C. L. Tan, I. Poschke, E. Green, S. Justesen, G. A. Behrens, M. O. Breckwoldt, A. Freitag, L.-M. Rother, A. Schmitt, O. Schnell, J. Hense, M. Misch, D. Krex, S. Stevanovic, G. Tabatabai, J. P. Steinbach, M. Bendszus, A. von Deimling, M. Schmitt, W. Wick, A vaccine targeting mutant IDH1 in newly diagnosed glioma. *Nature* **592**, 463-468 (2021).

14. M. R. Gilbert, Y. Liu, J. Neltner, H. Pu, A. Morris, M. Sunkara, T. Pittman, N. Kyprianou, C. Horbinski, Autophagy and oxidative stress in gliomas with IDH1 mutations. *Acta Neuropathologica* **127**, 221-233 (2014).

15. J. Núñez Felipe, M. Mendez Flor, P. Kadiyala, S. Alghamri Mahmoud, G. Savelieff Masha, B. Garcia-Fabiani Maria, S. Haase, C. Koschmann, A.-A. Calinescu, N. Kamran, M. Saxena, R. Patel, S. Carney, Z. Guo Marissa, M. Edwards, M. Ljungman, T. Qin, A. Sartor Maureen, R. Tagett, S. Venneti, J. Brosnan-Cashman, A. Meeker, V. Gorbunova, L. Zhao, M. Kremer Daniel, L. Zhang, A. Lyssiotis Costas, L. Jones, J. Herting Cameron, L. Ross James, D. Hambardzumyan, S. Hervey-Jumper, E. Figueroa Maria, R. Lowenstein Pedro, G. Castro Maria, IDH1-R132H acts as a tumor suppressor in glioma via epigenetic up-regulation of the DNA damage response. *Science Translational Medicine* **11**, eaaq1427 (2019).

16. M. Garrett, J. Sperry, D. Braas, W. Yan, T. M. Le, J. Mottahedeh, K. Ludwig, A. Eskin, Y. Qin, R. Levy, J. J. Breunig, F. Pajonk, T. G. Graeber, C. G. Radu, H. Christofk, R. M. Prins, A. Lai, L. M. Liau, G. Coppola, H. I. Kornblum, Metabolic characterization of isocitrate dehydrogenase (IDH) mutant and IDH wildtype gliomaspheres uncovers cell type-specific vulnerabilities. *Cancer & Metabolism* **6**, 4 (2018).

17. S. Ohba, J. Mukherjee, W. L. See, R. O. Pieper, Mutant IDH1-Driven Cellular Transformation Increases RAD51-Mediated Homologous Recombination and Temozolomide Resistance. *Cancer Research* **74**, 4836-4844 (2014).

18. S. V. Carney, K. Banerjee, A. Mujeeb, B. Zhu, S. Haase, M. L. Varela, P. Kadiyala, C. Tronrud, Z. Zhu, D. Mukherji, P. Gorla, R. Tagett, F. J. Núñez, M. Luo, W. Lou, M. Ljungman, Y. Liu, Z. Xia, A. Schwendeman, T. Qin, M. A. Sartor, J. Costello, D. P. Cahill, P. R. Lowenstein, M. G. Castro, Zinc Finger MYND-Type Containing 8 (ZMYND8) is epigenetically regulated in mutant Isocitrate Dehydrogenase 1 (IDH1) glioma to promote radioresistance. *bioRxiv*, 2022.2006.2010.495694 (2022).

19. Z. J. Reitman, C. G. Duncan, E. Poteet, A. Winters, L.-J. Yan, D. M. Gooden, I. Spasojevic, L. G. Boros, S.-H. Yang, H. Yan, Cancer-associated Isocitrate Dehydrogenase 1 (IDH1) R132H Mutation and d-2-Hydroxyglutarate Stimulate Glutamine Metabolism under Hypoxia*. *Journal of Biological Chemistry* **289**, 23318-23328 (2014).

20. J. L. Izquierdo-Garcia, P. Viswanath, P. Eriksson, L. Cai, M. Radoul, M. M. Chaumeil, M. Blough, H. A. Luchman, S. Weiss, J. G. Cairncross, J. J. Phillips, R. O. Pieper, S. M. Ronen, IDH1 Mutation Induces Reprogramming of Pyruvate Metabolism. *Cancer Research* **75**, 2999-3009 (2015).
21. M. S. Waitkus, C. J. Pirozzi, C. J. Moure, B. H. Diplas, L. J. Hansen, A. B. Carpenter, R. Yang, Z. Wang, B. O. Ingram, E. D. Karoly, R. P. Mohney, I. Spasojevic, R. E. McLendon, H. S. Friedman, Y. He, D. D. Bigner, H. Yan, Adaptive Evolution of the GDH2 Allosteric Domain Promotes Gliomagenesis by Resolving IDH1R132H-Induced Metabolic Liabilities. *Cancer Research* **78**, 36-50 (2018).
22. P. Kadiyala, S. V. Carney, J. C. Gauss, M. B. Garcia-Fabiani, S. Haase, M. S. Alghamri, F. J. Núñez, Y. Liu, M. Yu, A. Taher, F. M. Nunez, D. Li, M. B. Edwards, C. G. Kleer, H. Appelman, Y. Sun, L. Zhao, J. J. Moon, A. Schwendeman, P. R. Lowenstein, M. G. Castro, Inhibition of 2-hydroxyglutarate elicits metabolic reprogramming and mutant IDH1 glioma immunity in mice. *The Journal of Clinical Investigation* **131**, (2021).
23. S. Miyata, K. Tominaga, E. Sakashita, M. Urabe, Y. Onuki, A. Gomi, T. Yamaguchi, M. Mieno, H. Mizukami, A. Kume, K. Ozawa, E. Watanabe, K. Kawai, H. Endo, Comprehensive Metabolomic Analysis of IDH1R132H Clinical Glioma Samples Reveals Suppression of β-oxidation Due to Carnitine Deficiency. *Scientific Reports* **9**, 9787 (2019).
24. L. Zhou, Z. Wang, C. Hu, C. Zhang, P. Kovatcheva-Datchary, D. Yu, S. Liu, F. Ren, X. Wang, Y. Li, X. Hou, H. Piao, X. Lu, Y. Zhang, G. Xu, Integrated Metabolomics and Lipidomics Analyses Reveal Metabolic Reprogramming in Human Glioma with IDH1 Mutation. *Journal of Proteome Research* **18**, 960-969 (2019).
25. D. A. N Mustafa, S. M. Swagemakers, L. Buise, P. J. van der Spek, J. M. Kros, Metabolic alterations due to IDH1 mutation in glioma: opening for therapeutic opportunities? *Acta Neuropathologica Communications* **2**, 6 (2014).
26. Caroline A. Lewis, Seth J. Parker, Brian P. Fiske, D. McCloskey, Dan Y. Gui, Courtney R. Green, Natalie I. Vokes, Adam M. Feist, Matthew G. Vander Heiden, Christian M. Metallo, Tracing Compartmentalized NADPH Metabolism in the Cytosol and Mitochondria of Mammalian Cells. *Molecular Cell* **55**, 253-263 (2014).
27. I. V. Mohrenz, P. Antonietti, S. Pusch, D. Capper, J. Balss, S. Voigt, S. Weissert, A. Mukrowsky, J. Frank, C. Senft, V. Seifert, A. von Deimling, D. Kögel, Isocitrate dehydrogenase 1 mutant R132H sensitizes glioma cells to BCNU-induced oxidative stress and cell death. *Apoptosis* **18**, 1416-1425 (2013).
28. J. Shi, B. Sun, W. Shi, H. Zuo, D. Cui, L. Ni, J. Chen, Decreasing GSH and increasing ROS in chemosensitivity gliomas with IDH1 mutation. *Tumor Biology* **36**, 655-662 (2015).
29. M. Khurshed, N. Aarnoudse, R. Hulsbos, V. V. V. Hira, H. W. M. van Laarhoven, J. W. Wilmink, R. J. Molenaar, C. J. F. van Noorden, IDH1-mutant cancer cells are sensitive to cisplatin and an IDH1-mutant inhibitor counteracts this sensitivity. *The FASEB Journal* **32**, 6344-6352 (2018).
30. J. Biedermann, M. Preussler, M. Conde, M. Peitzsch, S. Richter, R. Wiedemuth, K. Abou-El-Ardat, A. Krüger, M. Meinhardt, G. Schackert, W. P. Leenders, C. Herold-Mende, S. P. Niclou, R. Bjerkvig, G. Eisenhofer, A. Temme, M. Seifert, L. A. Kunz-Schughart, E. Schröck, B. Klink, Mutant IDH1 Differently Affects Redox State and Metabolism in Glial Cells of Normal and Tumor Origin. *Cancers* **11**, (2019).
31. E. White, Deconvoluting the context-dependent role for autophagy in cancer. *Nature Reviews Cancer* **12**, 401-410 (2012).
32. J. D. Rabinowitz, E. White, Autophagy and Metabolism. *Science* **330**, 1344-1348 (2010).
33. A. N. Hale, D. J. Ledbetter, T. R. Gawriluk, I. I. I. E. B. Rucker, Autophagy. *Autophagy* **9**, 951-972 (2013).
34. X. Li, S. He, B. Ma, Autophagy and autophagy-related proteins in cancer. *Molecular Cancer* **19**, 12 (2020).

35. B. V. Houten, S. E. Hunter, J. N. Meyer, Mitochondrial DNA damage induced autophagy, cell death, and disease. *FBL* **21**, 42-54 (2016).
36. A. G. Eliopoulos, S. Havaki, V. G. Gorgoulis, DNA Damage Response and Autophagy: A Meaningful Partnership. *Frontiers in Genetics* **7**, (2016).
37. A. Ianniciello, K. M. Rattigan, G. V. Helgason, The Ins and Outs of Autophagy and Metabolism in Hematopoietic and Leukemic Stem Cells: Food for Thought. *Frontiers in Cell and Developmental Biology* **6**, (2018).
38. R. A. Nixon, The role of autophagy in neurodegenerative disease. *Nature Medicine* **19**, 983-997 (2013).
39. C. D. Gonzalez, M.-S. Lee, P. Marchetti, M. Pietropaolo, R. Towns, M. I. Vaccaro, H. Watada, J. W. Wiley, The emerging role of autophagy in the pathophysiology of diabetes mellitus. *Autophagy* **7**, 2-11 (2011).
40. E. White, The role for autophagy in cancer. *The Journal of Clinical Investigation* **125**, 42-46 (2015).
41. S. S. Singh, S. Vats, A. Y.-Q. Chia, T. Z. Tan, S. Deng, M. S. Ong, F. Arfuso, C. T. Yap, B. C. Goh, G. Sethi, R. Y.-J. Huang, H. M. Shen, R. Manjithaya, A. P. Kumar, Dual role of autophagy in hallmarks of cancer. *Oncogene* **37**, 1142-1158 (2018).
42. P. Viswanath, M. Radoul, J. L. Izquierdo-Garcia, W. Q. Ong, H. A. Luchman, J. G. Cairncross, B. Huang, R. O. Pieper, J. J. Phillips, S. M. Ronen, 2-Hydroxyglutarate-Mediated Autophagy of the Endoplasmic Reticulum Leads to an Unusual Downregulation of Phospholipid Biosynthesis in Mutant IDH1 Gliomas. *Cancer Research* **78**, 2290-2304 (2018).
43. M. S. Alghamri, K. Banerjee, A. A. Mujeeb, A. Mauser, A. Taher, R. Thalla, B. L. McClellan, M. L. Varela, S. M. Stamatovic, G. Martinez-Revollar, A. V. Andjelkovic, J. V. Gregory, P. Kadiyala, A. Calinescu, J. A. Jiménez, A. A. Apfelbaum, E. R. Lawlor, S. Carney, A. Comba, S. M. Faisal, M. Barissi, M. B. Edwards, H. Appelman, Y. Sun, J. Gan, R. Ackermann, A. Schwendeman, M. Candolfi, M. R. Olin, J. Lahann, P. R. Lowenstein, M. G. Castro, Systemic Delivery of an Adjuvant CXCR4–CXCL12 Signaling Inhibitor Encapsulated in Synthetic Protein Nanoparticles for Glioma Immunotherapy. *ACS Nano* **16**, 8729-8750 (2022).
44. J. V. Gregory, P. Kadiyala, R. Doherty, M. Cadena, S. Habeel, E. Ruoslahti, P. R. Lowenstein, M. G. Castro, J. Lahann, Systemic brain tumor delivery of synthetic protein nanoparticles for glioblastoma therapy. *Nature Communications* **11**, 5687 (2020).
45. D. Grasso, F. J. Renna, M. I. Vaccaro, Initial Steps in Mammalian Autophagosome Biogenesis. *Frontiers in Cell and Developmental Biology* **6**, (2018).
46. C. Di Malta, L. Cinque, C. Settembre, Transcriptional Regulation of Autophagy: Mechanisms and Diseases. *Frontiers in Cell and Developmental Biology* **7**, (2019).
47. J. A. Losman, W. G. Kaelin, Jr., What a difference a hydroxyl makes: mutant IDH, (R)-2-hydroxyglutarate, and cancer. *Genes Dev* **27**, 836-852 (2013).
48. S. K. McBrayer, J. R. Mayers, G. J. DiNatale, D. D. Shi, J. Khanal, A. A. Chakraborty, K. A. Sarosiek, K. J. Briggs, A. K. Robbins, T. Sewastianik, S. J. Shareef, B. A. Olenchock, S. J. Parker, K. Tateishi, J. B. Spinelli, M. Islam, M. C. Haigis, R. E. Looper, K. L. Ligon, B. E. Bernstein, R. D. Carrasco, D. P. Cahill, J. M. Asara, C. M. Metallo, N. H. Yennawar, M. G. Vander Heiden, W. G. Kaelin, Jr., Transaminase Inhibition by 2-Hydroxyglutarate Impairs Glutamate Biosynthesis and Redox Homeostasis in Glioma. *Cell* **175**, 101-116.e125 (2018).
49. R. J. Youle, A. M. van der Bliek, Mitochondrial Fission, Fusion, and Stress. *Science* **337**, 1062-1065 (2012).
50. J. L. Burman, S. Pickles, C. Wang, S. Sekine, J. N. S. Vargas, Z. Zhang, A. M. Youle, C. L. Nezich, X. Wu, J. A. Hammer, R. J. Youle, Mitochondrial fission facilitates the selective mitophagy of protein aggregates. *Journal of Cell Biology* **216**, 3231-3247 (2017).
51. S. Zhao, Y. Lin, W. Xu, W. Jiang, Z. Zha, P. Wang, W. Yu, Z. Li, L. Gong, Y. Peng, J. Ding, Q. Lei, K.-L. Guan, Y. Xiong, Glioma-Derived Mutations in IDH1 Dominantly Inhibit IDH1 Catalytic Activity and Induce HIF-1α. *Science* **324**, 261-265 (2009).

52. T. Huang, C. K. Kim, A. A. Alvarez, R. P. Pangeni, X. Wan, X. Song, T. Shi, Y. Yang, N. Sastry, C. M. Horbinski, S. Lu, R. Stupp, J. A. Kessler, R. Nishikawa, I. Nakano, E. P. Sulman, X. Lu, C. D. James, X.-M. Yin, B. Hu, S.-Y. Cheng, MST4 Phosphorylation of ATG4B Regulates Autophagic Activity, Tumorigenicity, and Radioresistance in Glioblastoma. *Cancer Cell* **32**, 840-855.e848 (2017).
53. I. Tanida, T. Ueno, E. Kominami, in *Autophagosome and Phagosome,* V. Deretic, Ed. (Humana Press, Totowa, NJ, 2008), pp. 77-88.
54. W. W.-Y. Yim, N. Mizushima, Lysosome biology in autophagy. *Cell Discovery* **6**, 6 (2020).
55. D. S. Leeman, K. Hebestreit, T. Ruetz, A. E. Webb, A. McKay, E. A. Pollina, B. W. Dulken, X. Zhao, R. W. Yeo, T. T. Ho, S. Mahmoudi, K. Devarajan, E. Passegué, T. A. Rando, J. Frydman, A. Brunet, Lysosome activation clears aggregates and enhances quiescent neural stem cell activation during aging. *Science* **359**, 1277-1283 (2018).
56. H. Chaachouay, P. Ohneseit, M. Toulany, R. Kehlbach, G. Multhoff, H. P. Rodemann, Autophagy contributes to resistance of tumor cells to ionizing radiation. *Radiotherapy and Oncology* **99**, 287-292 (2011).
57. K. Masui, H. Onizuka, W. K. Cavenee, P. S. Mischel, N. Shibata, Metabolic reprogramming in the pathogenesis of glioma: Update. *Neuropathology* **39**, 3-13 (2019).
58. A. R. Grassian, S. J. Parker, S. M. Davidson, A. S. Divakaruni, C. R. Green, X. Zhang, K. L. Slocum, M. Pu, F. Lin, C. Vickers, C. Joud-Caldwell, F. Chung, H. Yin, E. D. Handly, C. Straub, J. D. Growney, M. G. Vander Heiden, A. N. Murphy, R. Pagliarini, C. M. Metallo, IDH1 Mutations Alter Citric Acid Cycle Metabolism and Increase Dependence on Oxidative Mitochondrial Metabolism. *Cancer Research* **74**, 3317-3331 (2014).
59. F. Fack, S. Tardito, G. Hochart, A. Oudin, L. Zheng, S. Fritah, A. Golebiewska, P. V. Nazarov, A. Bernard, A.-C. Hau, O. Keunen, W. Leenders, M. Lund-Johansen, J. Stauber, E. Gottlieb, R. Bjerkvig, S. P. Niclou, Altered metabolic landscape in IDH-mutant gliomas affects phospholipid, energy, and oxidative stress pathways. *EMBO Molecular Medicine* **9**, 1681-1695 (2017).
60. G. Karpel-Massler, C. T. Ishida, E. Bianchetti, Y. Zhang, C. Shu, T. Tsujiuchi, M. A. Banu, F. Garcia, K. A. Roth, J. N. Bruce, P. Canoll, M. D. Siegelin, Induction of synthetic lethality in IDH1-mutated gliomas through inhibition of Bcl-xL. *Nature Communications* **8**, 1067 (2017).
61. P. López de Figueroa, M. K. Lotz, F. J. Blanco, B. Caramés, Autophagy Activation and Protection From Mitochondrial Dysfunction in Human Chondrocytes. *Arthritis & Rheumatology* **67**, 966-976 (2015).
62. B. Zhao, L. Qiang, J. Joseph, B. Kalyanaraman, B. Viollet, Y.-Y. He, Mitochondrial dysfunction activates the AMPK signaling and autophagy to promote cell survival. *Genes & Diseases* **3**, 82-87 (2016).
63. D. H. Youn, Y. Kim, B. J. Kim, M. S. Jeong, J. Lee, J. K. Rhim, H. C. Kim, J. P. Jeon, Mitochondrial dysfunction associated with autophagy and mitophagy in cerebrospinal fluid cells of patients with delayed cerebral ischemia following subarachnoid hemorrhage. *Scientific Reports* **11**, 16512 (2021).
64. A. H. Tang, T. A. Rando, Induction of autophagy supports the bioenergetic demands of quiescent muscle stem cell activation. *The EMBO Journal* **33**, 2782-2797 (2014).
65. D. J. Klionsky, H. Abeliovich, P. Agostinis, D. K. Agrawal, G. Aliev, D. S. Askew, M. Baba, E. H. Baehrecke, B. A. Bahr, A. Ballabio, B. A. Bamber, D. C. Bassham, E. Bergamini, X. Bi, M. Biard-Piechaczyk, J. S. Blum, D. E. Bredesen, J. L. Brodsky, J. H. Brumell, U. T. Brunk, W. Bursch, N. Camougrand, E. Cebollero, F. Cecconi, Y. Chen, L.-S. Chin, A. Choi, C. T. Chu, J. Chung, R. S. B. Clark, P. G. H. Clarke, S. G. Clarke, C. Clave, J. L. Cleveland, P. Codogno, M. I. Colombo, A. Coto-Montes, J. M. Cregg, A. M. Cuervo, J. Debnath, P. B. Dennis, P. A. Dennis, F. Demarchi, V. Deretic, R. J. Devenish, F. Di Sano, J. F. Dice, C. W. Distelhorst, S. P. Dinesh-Kumar, N. T. Eissa, M. DiFiglia, M. Djavaheri-Mergny, F. C. Dorsey, W. Dröge, M. Dron, J. W. A. Dunn, M. Duszenko, Z. Elazar, A. Esclatine, E.-L. Eskelinen, L. Fésüs, K. D. Finley, J. M. Fuentes, J. Fueyo-

Margareto, K. Fujisaki, B. Galliot, F.-B. Gao, D. A. Gewirtz, S. B. Gibson, A. Gohla, A. L. Goldberg, R. Gonzalez, C. González-Estévez, S. M. Gorski, R. A. Gottlieb, D. Häussinger, Y.-W. He, K. Heidenreich, J. A. Hill, M. Høyer-Hansen, X. Hu, W.-P. Huang, A. Iwasaki, M. Jäättelä, W. T. Jackson, X. Jiang, S. V. Jin, T. Johansen, J. U. Jung, M. Kadowaki, C. Kang, A. Kelekar, D. H. Kessel, J. A. K. W. Kiel, H. P. Kim, A. Kimchi, T. J. Kinsella, K. Kiselyov, K. Kitamoto, E. Knecht, M. Komatsu, E. Kominami, S. Kondo, A. L. Kovács, G. Kroemer, C.-Y. Kuan, R. Kumar, M. Kundu, J. Landry, M. Laporte, W. Le, H.-Y. Lei, B. Levine, A. P. Lieberman, K.-L. Lim, F.-C. Lin, W. Liou, L. F. Liu, G. Lopez-Berestein, C. López-Otín, B. Lu, K. F. Macleod, W. Malorni, W. Martinet, K. Matsuoka, J. Mautner, A. J. Meijer, A. Meléndez, P. Michels, G. Miotto, W. P. Mistiaen, N. Mizushima, B. Mograbi, M. N. Moore, P. I. Moreira, Y. Moriyasu, T. Motyl, C. Münz, L. O. Murphy, N. I. Naqvi, T. P. Neufeld, I. Nishino, R. A. Nixon, T. Noda, B. Nürnberg, M. Ogawa, N. L. Oleinick, L. J. Olsen, B. Ozpolat, S. Paglin, G. E. Palmer, I. S. Papassideri, M. Parkes, D. H. Perlmutter, G. Perry, M. Piacentini, R. Pinkas-Kramarski, M. Prescott, T. Proikas-Cezanne, N. Raben, A. Rami, F. Reggiori, B. Rohrer, D. C. Rubinsztein, K. M. Ryan, J. Sadoshima, H. Sakagami, Y. Sakai, M. Sandri, C. Sasakawa, M. Sass, C. Schneider, P. O. Seglen, O. Seleverstov, J. Settleman, J. J. Shacka, I. M. Shapiro, A. A. Sibirny, E. C. M. Silva-Zacarin, H.-U. Simon, C. Simone, A. Simonsen, M. A. Smith, K. Spanel-Borowski, V. Srinivas, M. Steeves, H. Stenmark, P. E. Stromhaug, C. S. Subauste, S. Sugimoto, D. Sulzer, T. Suzuki, M. S. Swanson, I. Tabas, F. Takeshita, N. J. Talbot, Z. Tallóczy, K. Tanaka, K. Tanaka, I. Tanida, G. S. Taylor, J. P. Taylor, A. Terman, G. Tettamanti, C. B. Thompson, M. Thumm, A. M. Tolkovsky, S. A. Tooze, R. Truant, L. V. Tumanovska, Y. Uchiyama, T. Ueno, N. L. Uzcátegui, I. J. van der Klei, E. C. Vaquero, T. Vellai, M. W. Vogel, H.-G. Wang, P. Webster, Z. Xi, G. Xiao, J. Yahalom, J.-M. Yang, G. S. Yap, X.-M. Yin, T. Yoshimori, Z. Yue, M. Yuzaki, O. Zabirnyk, X. Zheng, X. Zhu, R. L. Deter, Guidelines for the use and interpretation of assays for monitoring autophagy in higher eukaryotes. *Autophagy* **4**, 151-175 (2008).

66. L. Poillet-Perez, J.-E. Sarry, C. Joffre, Autophagy is a major metabolic regulator involved in cancer therapy resistance. *Cell Reports* **36**, 109528 (2021).

67. Q.-W. Fan, C. Cheng, C. Hackett, M. Feldman, B. T. Houseman, T. Nicolaides, D. Haas-Kogan, C. D. James, S. A. Oakes, J. Debnath, K. M. Shokat, W. A. Weiss, Akt and Autophagy Cooperate to Promote Survival of Drug-Resistant Glioma. *Science Signaling* **3**, ra81-ra81 (2010).

68. Y. Yan, Z. Xu, S. Dai, L. Qian, L. Sun, Z. Gong, Targeting autophagy to sensitive glioma to temozolomide treatment. *Journal of Experimental & Clinical Cancer Research* **35**, 23 (2016).

69. M. L. Bristol, S. M. Emery, P. Maycotte, A. Thorburn, S. Chakradeo, D. A. Gewirtz, Autophagy Inhibition for Chemosensitization and Radiosensitization in Cancer: Do the Preclinical Data Support This Therapeutic Strategy? *Journal of Pharmacology and Experimental Therapeutics* **344**, 544 (2013).

70. L. Mele, V. del Vecchio, D. Liccardo, C. Prisco, M. Schwerdtfeger, N. Robinson, V. Desiderio, V. Tirino, G. Papaccio, M. La Noce, The role of autophagy in resistance to targeted therapies. *Cancer Treatment Reviews* **88**, 102043 (2020).

71. A. Escamilla-Ramírez, R. A. Castillo-Rodríguez, S. Zavala-Vega, D. Jimenez-Farfan, I. Anaya-Rubio, E. Briseño, G. Palencia, P. Guevara, A. Cruz-Salgado, J. Sotelo, C. Trejo-Solís, Autophagy as a Potential Therapy for Malignant Glioma. *Pharmaceuticals* **13**, (2020).

72. R. Mathew, S. Kongara, B. Beaudoin, C. M. Karp, K. Bray, K. Degenhardt, G. Chen, S. Jin, E. White, Autophagy suppresses tumor progression by limiting chromosomal instability. *Genes Dev* **21**, 1367-1381 (2007).

73. S. G. Holdgaard, V. Cianfanelli, E. Pupo, M. Lambrughi, M. Lubas, J. C. Nielsen, S. Eibes, E. Maiani, L. M. Harder, N. Wesch, M. M. Foged, K. Maeda, F. Nazio, L. R. de la Ballina, V. Dötsch, A. Brech, L. B. Frankel, M. Jäättelä, F. Locatelli, M. Barisic, J. S. Andersen, S. Bekker-Jensen, A. H. Lund, V. V. Rogov, E. Papaleo, L. Lanzetti, D. De Zio, F. Cecconi, Selective

autophagy maintains centrosome integrity and accurate mitosis by turnover of centriolar satellites. *Nature Communications* **10**, 4176 (2019).

74. Z. Zhao, D. Ni, I. Ghozalli, S. D. Pirooz, B. Ma, C. Liang, UVRAG. *Autophagy* **8**, 1392-1393 (2012).

75. F. Mendez, P. Kadiyala, F. J. Nunez, S. Carney, F. M. Nunez, J. C. Gauss, R. Ravindran, S. Pawar, M. Edwards, M. B. Garcia-Fabiani, S. Haase, P. R. Lowenstein, M. G. Castro, Therapeutic Efficacy of Immune Stimulatory Thymidine Kinase and fms-like Tyrosine Kinase 3 Ligand (TK/Flt3L) Gene Therapy in a Mouse Model of High-Grade Brainstem Glioma. *Clinical Cancer Research* **26**, 4080-4092 (2020).

Acknowledgments: We thank Dr. J. Costello (UCSF) for providing the mIDH1 human glioma cells SF10602, which were a gift from the Dabbiere Family and funded by NIH/NCI R01CA244838; the COG Repository at the Health Science Center for providing the human glioma cells SJGBM2; and Dr. J. Ohlfest (University of Minnesota, deceased) for providing the SB model plasmids.

Funding:

National Institutes of Health/National Institute of Neurological Disorders & Stroke (NIH/NINDS) Grant R37-NS094804 (MGC)

National Institutes of Health/National Institute of Neurological Disorders & Stroke (NIH/NINDS) Grant R01-NS122165 (MGC)

National Institutes of Health/National Institute of Neurological Disorders & Stroke (NIH/NINDS) Grant R01-NS124167 (MGC, JL)

National Institutes of Health/National Institute of Neurological Disorders & Stroke (NIH/NINDS) Grant R21-NS123879-01 (MGC)

National Institute of Health/National Institute of Neurological Disorders & Stroke (NIH/NINDS) Grant R01NS122234 (PRL)

National Institute of Health/National Institute of Neurological Disorders & Stroke (NIH/NINDS) Grant R01-NS122378 (PRL)

The Pediatric Brain Tumor Foundation (MGC, PRL)

Leah's Happy Hearts Foundation (MGC, PRL)

Ian's Friends Foundation (IFF) (MGC, PRL)

Chad Tough Foundation (MGC, PRL)

Smiles for Sophie Forever Foundation (MGC, PRL)

National Science Foundation Graduate Research Fellowship Grant DGE 1256260 (AM)

NCI Cancer Center Support Grant 2P30CA46592 (MGC)

Rogel Cancer Center Faculty Scholar Award (MGC)

National Cancer Institute (NCI) Grant R01CA248160 (CAL)

National Cancer Institute (NCI) Grant R01CA244931 (CAL)

Author contributions:

Conceptualization: MGC, FJN

Methodology: All: FJN, KB, AAM, AM, CET, ZZ, AT, PK, SVC, MBGF, AC, MSA, BLM, SYF, ZCN, HSH, TQ, MAS, ML, SYC, HDP, PRL, JL, CAL, MGC

Investigation: All: FJN, KB, AAM, AM, CET, ZZ, AT, PK, SVC, MBGF, AC, MSA, BLM, SYF, ZCN, HSH, TQ, MAS, ML, SYC, HDP, PRL, JL, CAL, MGC

Visualization: All: FJN, KB, AAM, AM, CET, ZZ, AT, PK, SVC, MBGF, AC, MSA, BLM, SYF, ZCN, HSH, TQ, MAS, ML, SYC, HDP, PRL, JL, CAL, MGC

Funding acquisition: MGC, PRL, CAL, JL

Project administration: MGC

Supervision: MGC, PRL, CAL, JL

Writing – original draft: All: FJN, KB, AAM, AM, CET, ZZ, AT, PK, SVC, MBGF, AC, MSA, BLM, SYF, ZCN, HSH, TQ, MAS, ML, SYC, HDP, PRL, JL, CAL, MGC

Writing – review & editing: All: FJN, KB, AAM, AM, CET, ZZ, AT, PK, SVC, MBGF, AC, MSA, BLM, SYF, ZCN, HSH, TQ, MAS, ML, SYC, HDP, PRL, JL, CAL, MGC

Competing interests: In the past three years, C.A.L. has consulted for Astellas Pharmaceuticals, Odyssey Therapeutics, Third Rock Ventures, and T-Knife Therapeutics, and is an inventor on patents pertaining to Kras regulated metabolic pathways, redox control pathways in pancreatic cancer, and targeting the GOT1-ME1 pathway as a therapeutic

approach (US Patent No: 2015126580-A1, 05/07/2015; US Patent No: 20190136238, 05/09/2019; International Patent No: WO2013177426-A2, 04/23/2015). All other authors declare that there are no conflict of interest regarding the publication of this article.

Data and materials availability: There are no limitations on data availability. The ChIP-Seq dataset generated in this study can be acquired through NCBI's Gene Expression Omnibus (GEO) with identifier GSE99806. The RNA-Seq dataset generated in this study can be acquired through NCBI's Gene Expression Omnibus (GEO) with identifiers GSE94902, GSE94974, and GSE94975. The scRNA-Seq dataset generated in this study can be acquired through NCBI's Gene Expression Omnibus (GEO) with identifier GSE261042. All other data generated within this study are available via the supplementary data files; cells and plasmids will be freely distributed upon request from the corresponding author, Maria G Castro.

Figure 1. mIDH1 glioma has upregulated autophagy and disrupts mitochondrial metabolism.

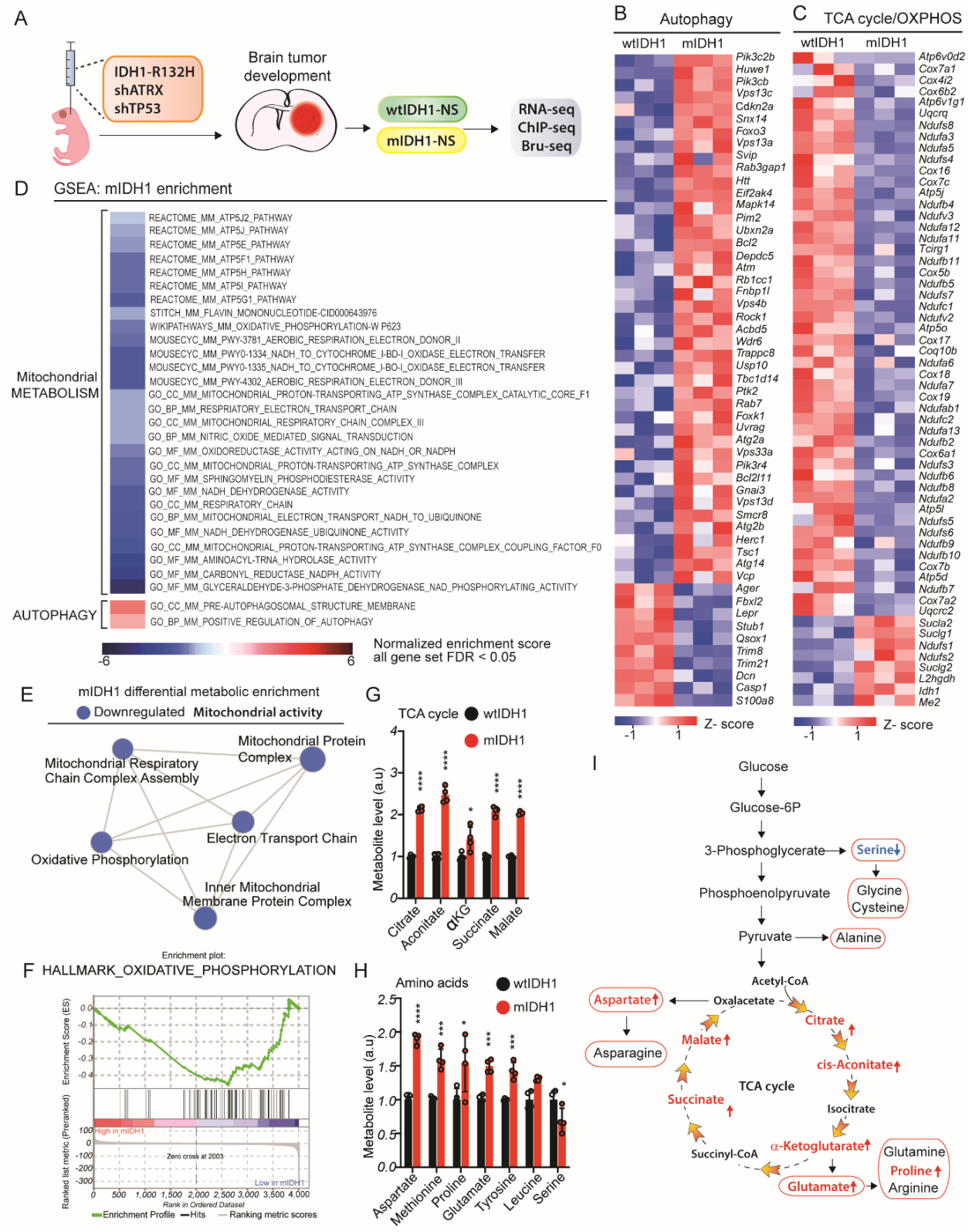

1

Fig. 1. mIDH1 glioma has upregulated autophagy and disrupts mitochondrial metabolism

(A) Illustration of genetically engineered mIDH1 glioma models harboring ATRX and TP53 knockdown and molecular analysis performed. **(B-C)** Heatmaps showing gene expression pattern for (B) autophagy and (C) electron transport chain (ETC) genes in wtIDH1-NS and mIDH1-NS (n=3 biological replicates; up-regulated genes are red; down-regulated genes are blue; FDR ≤ 0.05; ≥ 1.5-fold). **(D)** GSEA comparing transcriptional changes in mIDH1-NS versus wtIDH1–NS. Negative/positive normalized enrichment scores (blue/red scale; FDR < 0.05) show GO terms linked to metabolism (mitochondrial, OXPHOS) (downregulated) and autophagy (upregulated) in mIDH1-NS. **(E)** Pathway enrichment map of differentially enriched (DE) genes in mIDH1-NS versus wtIDH1–NS. Blue nodes illustrate down-regulation in mIDH1-NS (**P* < 0.05; overlap cutoff>0.5) related to mitochondrial metabolic activity. **(F)** Enrichment plots of gene sets significantly downregulated in mIDH1-NS with decreasing expression levels of OXPHOS genes detected by GSEA. Green curves show enrichment score and reflect degree of each gene (black lines) and is represented at bottom of ranked gene list. **(G-H)** Metabolomics profiling data showing relative levels of (G) tricarboxylic acid (TCA) cycle intermediates and (H) amino acid levels in wt and mIDH1-NS (a.u.: arbitrary unit). Results expressed as mean±SD.**P* < 0.05; ****P* < 0.001; *****P* < 0.0001; two-way ANOVA. **I)** Illustration showing TCA cycle intermediates and amino acids disrupted in mIDH1-NS versus wtIDH1-NS. Significantly altered amino acids depicted in red.

Figure 2. **Epigenetic reprogramming in mIDH1 glioma decreases metabolism and enhances autophagy in mIDH1 glioma cells.**

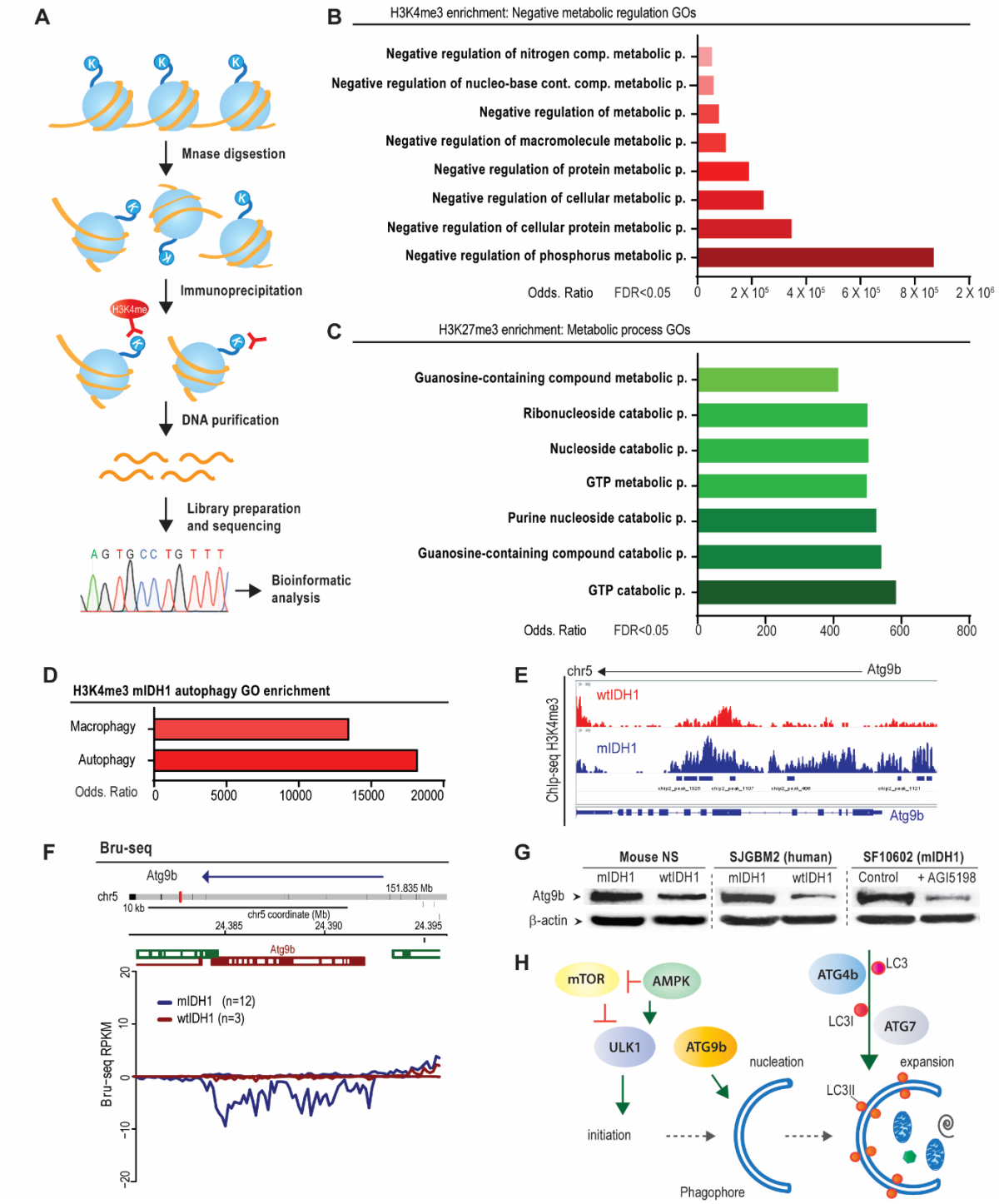

1

Fig. 2. Epigenetic reprogramming in mIDH1 glioma decreases metabolism and enhances autophagy in mIDH1 glioma cells. (A) Native ChIP-seq diagram performed on mIDH1-NS and wtIDH1-NS. (**B-D)** Genes enriched in H3K4me3 or H3K27me3 linked to distinct functional GO terms by ChIP-seq analysis. Bar graphs representing GO terms containing genes having enrichment of H3K4me3 (red) or H3K27me3 (green) at their promoter regions in mIDH1-NS. GO terms' significance determined by FDR (<0.05); enrichment expressed as odds ratio. (**E)** H3K4me3 occupancy in specific genomic regions of *Atg9b*. Y-axis represents estimated number of immunoprecipitated fragments normalized to total number of reads in each dataset. Reference sequence (RefSeq) gene annotations are shown. Differential peaks (FDR < 0.05) in wtIDH1–NS (red) versus mIDH1-NS (blue) (n=3 biological replicates per group). (**F)** Bru-Seq traces showing differential transcriptional rates (< 1.5-fold; $P < 0.05$) of *Atg9b* in mIDH1-NS (blue) versus wtIDH1–NS (red). Arrow indicates sequence strand reading direction; positive y-axis represents positive strand signal of transcription moving left to right; negative y-axis represents negative strand signal of transcription moving right to left. Vertical red mark indicates *Atg9b* position within chromosome. Genes and chromosome locations indicated on maps. Data expressed in reads per kilobase per million mapped reads (RPKM). Gene maps generated from RefSeq. (**G)** WB showing Atg9b protein expression in wtIDH1-NS, mIDH1-NS human glioma SJGBM2 wtIDH1 and mIDH1, and mIDH1 human glioma cells, SF10602, ±IDH1^{R132H} inhibitor AGI-5198 (5μM). (**H)** Diagram of initial steps of autophagy pathways, including phagophore formation with participation of Atg9b protein in the nucleation process.

Figure 3. **Epigenetic regulation of autophagy related genes involves histone methylation in mIDH1 human glioma cells.**

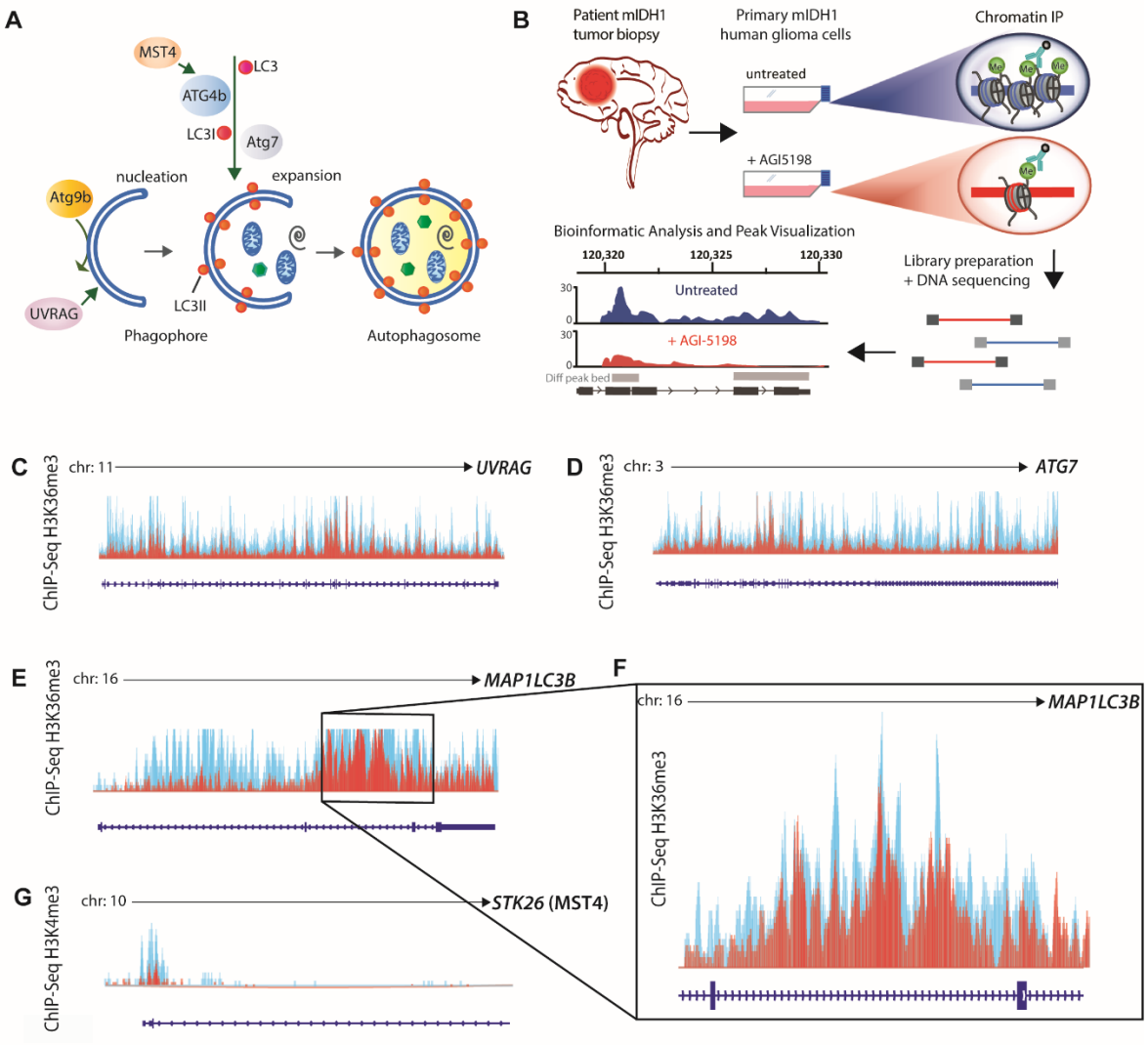

1

Fig. 3. Epigenetic regulation of autophagy related genes involves histone methylation in mIDH1 human glioma cells. (A) Diagram of autophagosome formation in the autophagic pathway involving autophagy related genes: UVRAG, ATG7, LC3 (*MAP1LC3B*), and MST4 (*STK26*). (**B)** Diagram of experimental design of ChIP-seq analysis performed in primary mIDH1 human glioma cells, SF10602, ±IDH1^{R132H} inhibitor AGI-5198 (5 µM), prior to chromatin immunoprecipitation (IP). (**C-G)** (C-F) H3K36me3 and (G) H3K4me3 occupancy in specific genomic regions of autophagy related genes *UVRAG*, *ATG7*, *MAP1LC3B* (LC3), and *STK26* (MST4). The y-axis of each profile represents the estimated number of immunoprecipitated fragments at each position normalized to the total number of reads in each dataset. RefSeq gene annotations are shown. Differential peaks (FDR < 0.05) in untreated SF10602 mIDH1 glioma cells are represented in blue compared to AGI-5198 treated cells in red (n = 3 biological replicates per group).

Figure 4. **Single Cell RNA-seq shows an enhancement of autophagy in human mIDH1 glioma cells.**

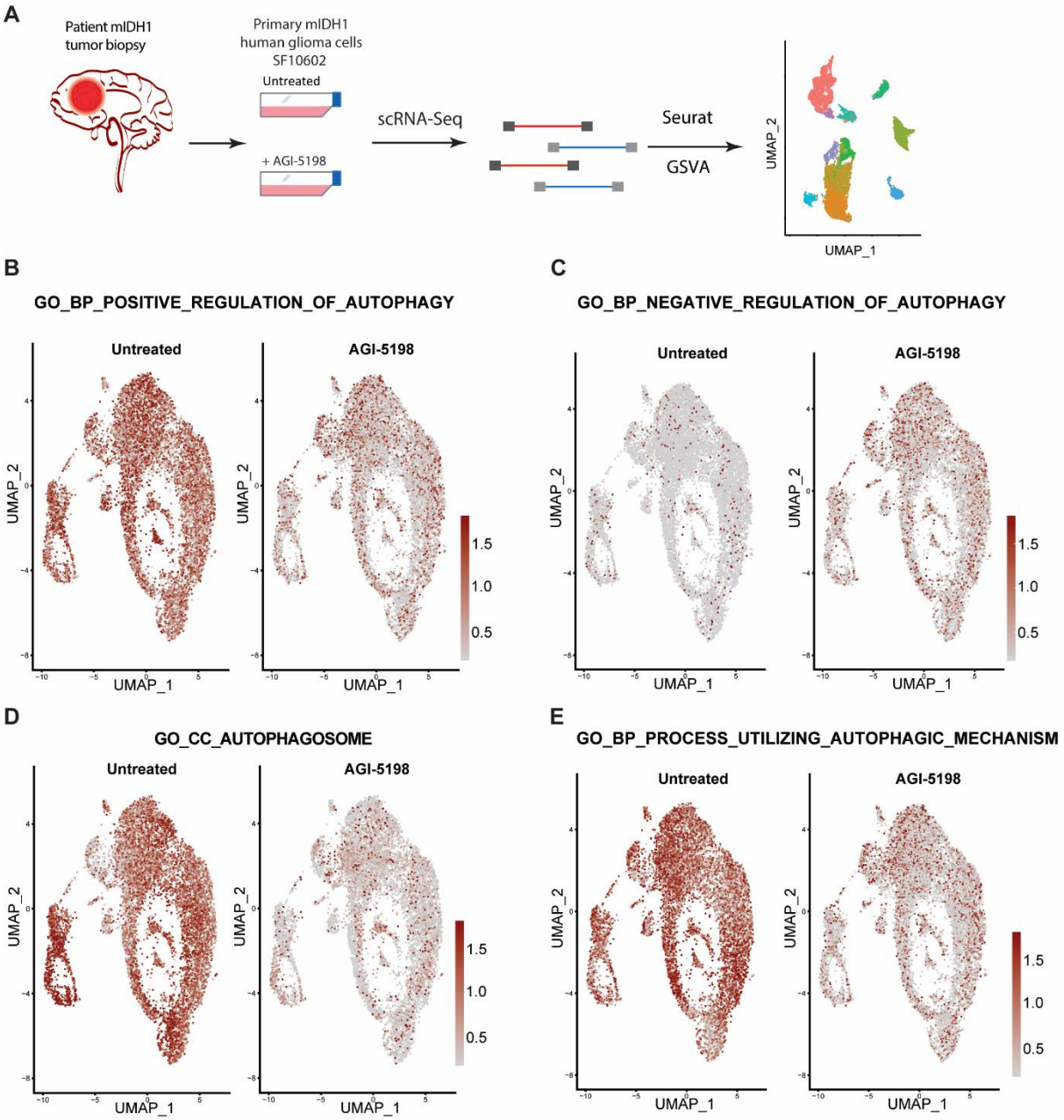

Fig. 4. Single Cell RNA-seq shows an enhancement of autophagy in human mIDH1 glioma cells. A) Diagram of experimental design of scRNA-seq analysis performed in primary mIDH1 human glioma cells, SF10602, ±IDH1^{R132H} inhibitor AGI-5198, prior to sequencing. **B)** GO term enrichment score for GO biological process of positive regulation of autophagy. **C)** GO term enrichment score for GO biological process of negative regulation of autophagy. **D)** GO term enrichment score for GO cellular component of autophagosome. **E)** GO term enrichment score for GO biological process of utilizing autophagic mechanism.

Figure 5. mIDH1 glioma cells show a quiescent state.

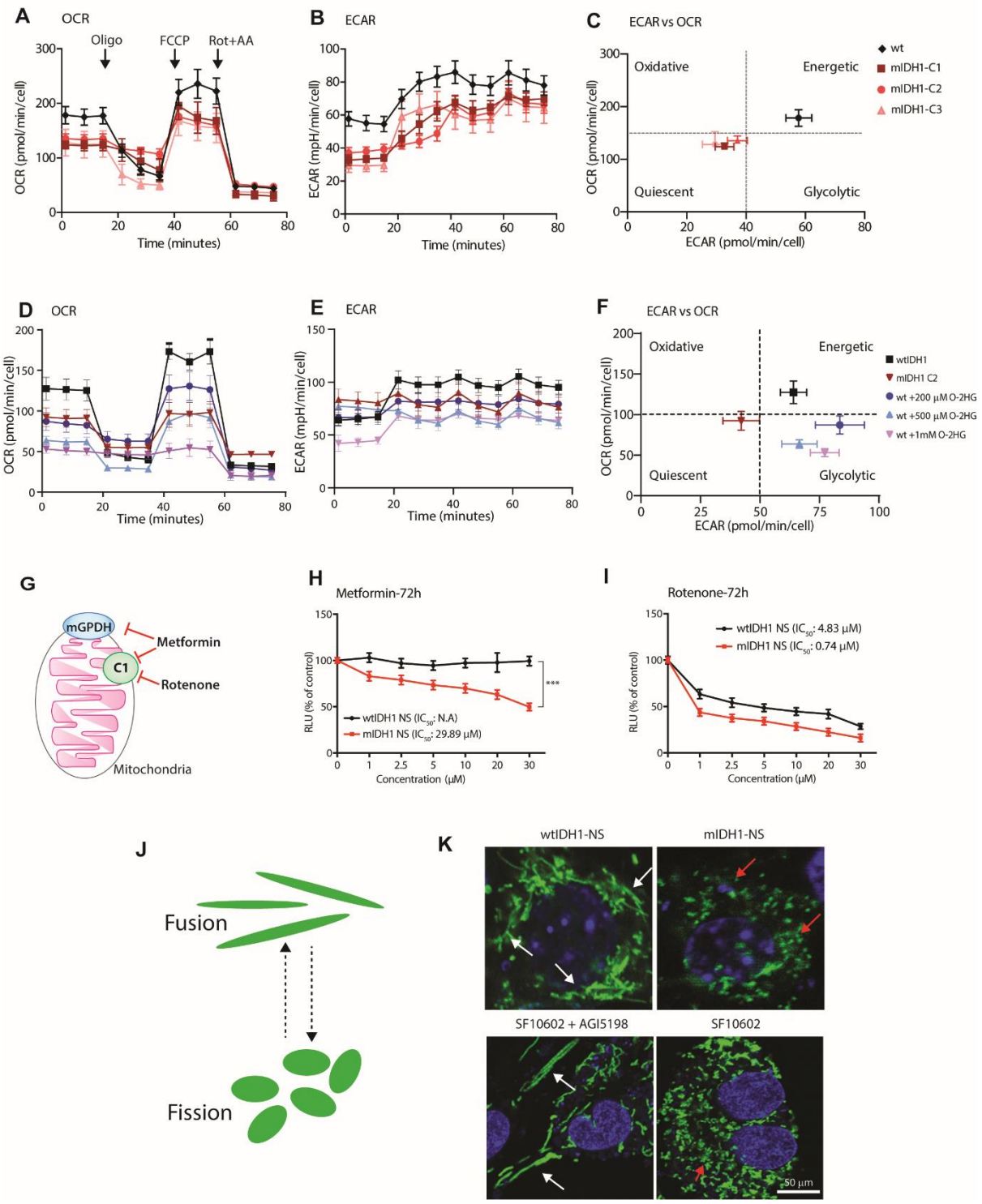

1

Fig. 5. mIDH1 glioma cells show a quiescent state (**A**) Mitochondrial respiration of glioma NS derived from wtIDH1 or mIDH1 tumors (Clones 1-3) examined through Mito Stress Test. Error bars depict SD of technical replicates from representative plot of 3 independent experiments. Mitochondrial respiration determined by oxygen consumption rates (OCR). (**B)** Glycolytic activity determined by extracellular acidification rates (ECAR) in mIDH1-NS and wtIDH1-NS. (**C)** Metabolic profile of wtIDH1-NS and mIDH1-NS comparing ECAR versus OCR. (**D)** Mito Stress Test performed on wtIDH1-NS, mIDH1-NS, and wtIDH1-NS cultured with cell-permeable (R)-2HG (wtIDH1-NS + O-2HG) for 4 hours at indicated concentrations. Error bars depict SD of technical replicates from representative plot of 3 independent experiments. (**E)** ECAR of wtIDH1-NS, mIDH1-NS, and wtIDH1-NS + O-2HG. (**F)** Metabolic profile of wtIDH1-NS, mIDH1-NS, and wtIDH1-NS + O-2HG, comparing ECAR versus OCR. Significance determined by one-way ANOVA. $*P < 0.05$, $**P < 0.01$, $***P < 0.001$, $****P < 0.0001$. (**G)** Diagram representing mitochondrial complex 1 (C1) inhibition by metformin and rotenone. (**H-I)** Cell viability assay of wtIDH1-NS and mIDH1-NS treated with (H) metformin and (I) rotenone for 72 hours at increasing concentrations. Cell viability expressed in relative luciferase units (RLU) in percent of control (100%). Linear regression model and generalized additive models (GAM) for flexible regression modeling were used to model dose-response relationship. $***P < 0.001$ (**J)** Diagram representing mitochondrial morphology: fusion (elongation) and fission (division). **(K)** Mitochondrial morphology observed with confocal microscopy in wtIDH1-NS, mIDH1-NS, and SF10602±AGI-5198, labeled with MitoTracker Green FM. White arrows indicate mitochondrial fusion; red arrows indicate mitochondrial fission.

Figure 6. **Enhanced autophagy actvity in mIDH1 glioma cells.**

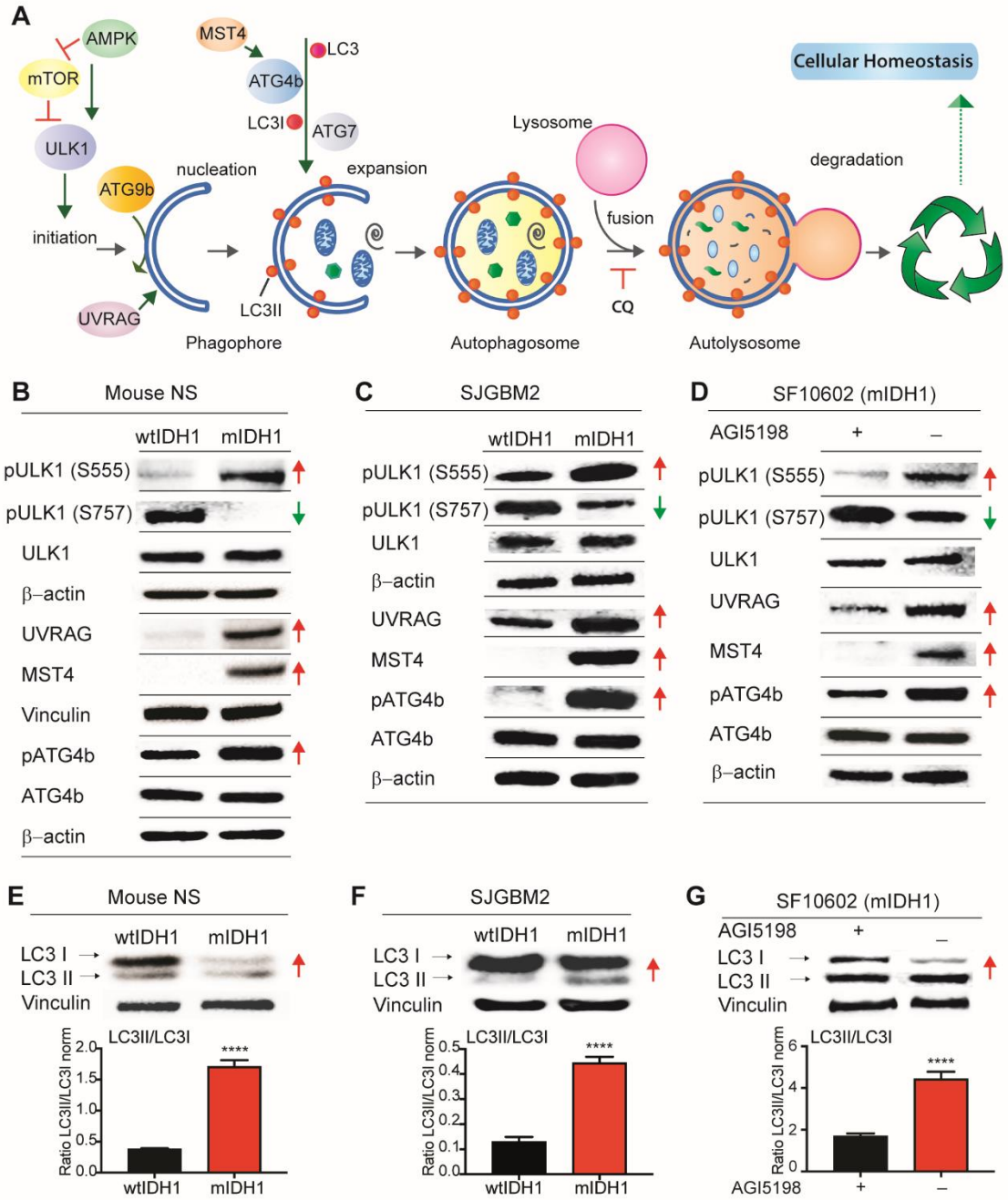

1

Fig. 6. Enhanced autophagy activity in mIDH1 glioma cells (A) The autophagy pathway is responsible for the recycling of cellular residues and damaged organelles thus maintaining hemostasis. This process includes initiation, expansion and degradation steps, where several proteins participate in the formation and transformation of the different cellular structures involved (phagophores, autophagosomes, lysosomes). (**B-D)** WB assay showing the expression of proteins involved in the autophagy pathways and the activated form of them, evaluated in (B) mIDH1and wtIDH1 mouse NS, (C) human glioma SJGBM2, and in (D) mIDH1 SF10602 mIDH1 human gliomas cells ± $IDH1^{R132H}$ inhibitor AGI-5198. The red arrows indicate the proteins and phosphorylated (p) status related with autophagy activation (pULK1 (S555), UVRAG, MST4, pATG4B (S383), whereas the green arrows indicate the phosphorylated (p) status related with autophagy inhibition (pULK1 (S757), β-actin and vinculin, loading control. (**E-F)** WB assay showing the conversion of LC3I to LC3II as indicator of autophagy activation (A). The increased ratio of LC3II/LC3I (red arrows) indicate autophagy activation. Vinculin is a loading control. Bar graph represents semi-quantification of WB assay (n = 3). ***P < 0.0001; T test. Bars represent means ± SEM (n = 3 technical replicates).

Figure 7. mIDH1 increases autophagy flux and *in vitro* inhibition of autophagy restores radiosensitivity in mIDH1 glioma cells

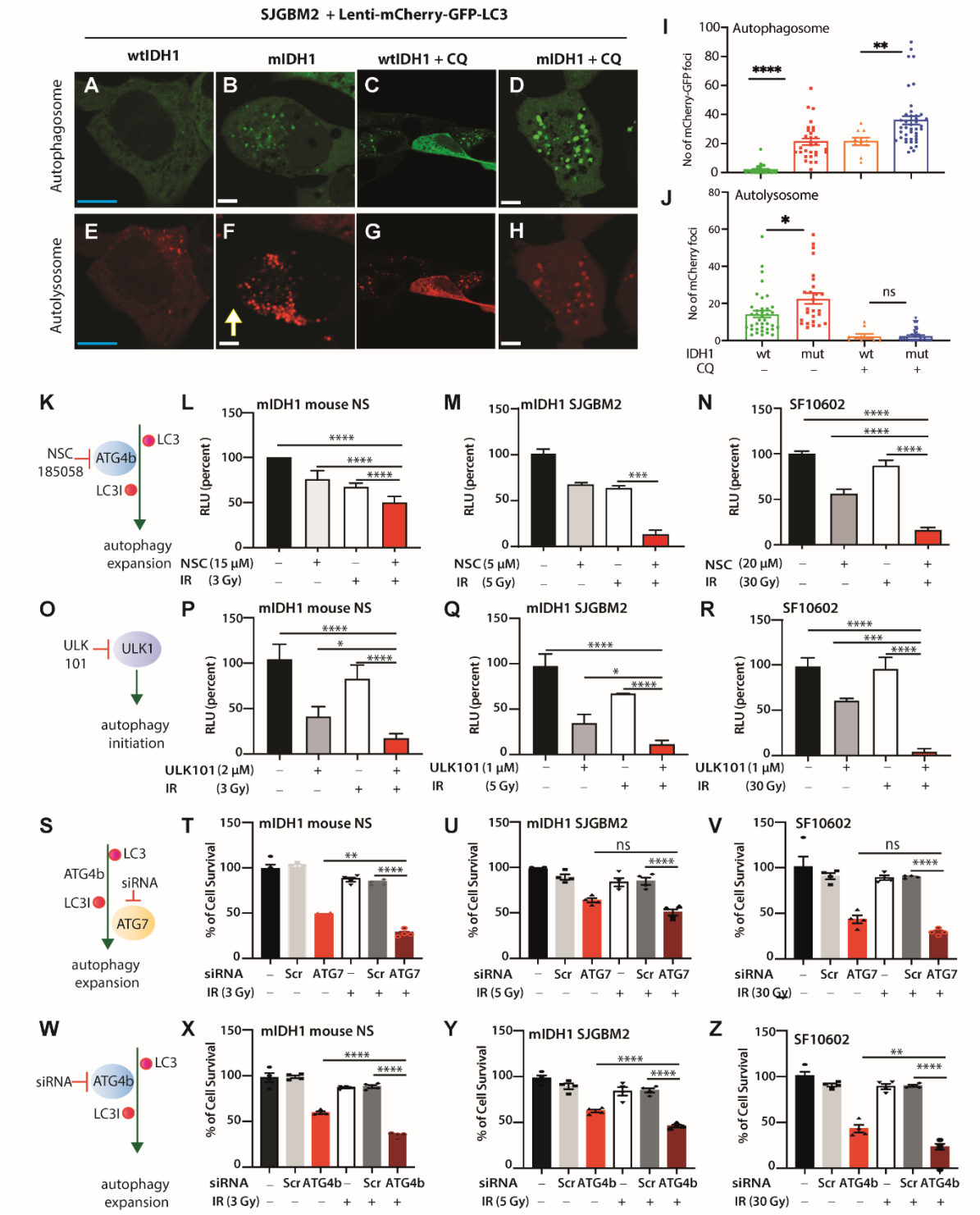

1

Fig. 7. mIDH1 increases autophagy flux and *in vitro* inhibition of autophagy restores radiosensitivity in mIDH1 glioma cells (**A-H)** Representative images of GFP and mCherry fluorescence in wt and mIDH1 human gliomas cells, SJGBM2, in basal condition or treated with 10 µM chloroquine (CQ). Scale Bar: 10 µm. (**I-J)** Quantification of number of (I) mCherry-GFP foci (indicating autophagosome formation) or (J) mCherry only foci (indicating autolysosome formation) in wt and mIDH1 SJGBM2 cells, in basal condition or treated with 10 µM chloroquine (CQ). Bar graphs represent the average of total foci per cell means ± SEM (n ≤ 10 replicates). $**P < 0.01$; $***P < 0.001$; One-way ANOVA followed by Tukey's test. **(K)** NSC-185058 compound inhibits Atg4b, which is involved in LC3 processing during autophagosome expansion. (**L-N)** Cell viability assay performed in (L) mIDH1 mouse and (M) human glioma cells, SJGBM2 and (N) SF10602 treated with indicated doses of NSC-185058 and ionizing radiation (IR). (**O)** ULK101 compound inhibits ULK1 during autophagy initiation. (**P-R)** Cell viability assay performed in (P) mIDH1 mouse and (Q) human glioma cells, SJGBM2 and (R) SF10602 treated with indicated doses of ULK101 and IR. Results are expressed in percent of RLU in relation with the untreated control (100 %). $*P < 0.05$; $**P < 0.01$ $***P < 0.001$; $****P < 0.0001$; One-way ANOVA followed by Tukey's test (n=4 technical replicates). (**S**) ATG7 inhibition by siRNA (siATG7) during autophagy initiation. (**T-V)** Cell viability assay performed in (T) mIDH1 mouse and (U) human glioma cells, SJGBM2 and (V) SF10602 treated with siATG7, and IR. Results are expressed in percent of cell survival in relation with the untreated control (100 %). (**W**) ATG4 inhibition by siRNA (siATG4) during autophagy initiation. (**X-Z)** Cell viability assay performed in (X) mIDH1 mouse and (Y) human glioma cells, SJGBM2 and (Z) SF10602 treated with siATG7, and IR. Results are expressed in percent of cell survival in relation with the untreated control (100 %). $*P < 0.05$; $**P < 0.01$ $***P < 0.001$; $****P < 0.0001$; One-way ANOVA followed by Tukey's test (n=4 technical replicates).

Figure 8. *In vivo* **inhibition of autophagy radiosensitizes mIDH1 gliomas and enhances survival.**

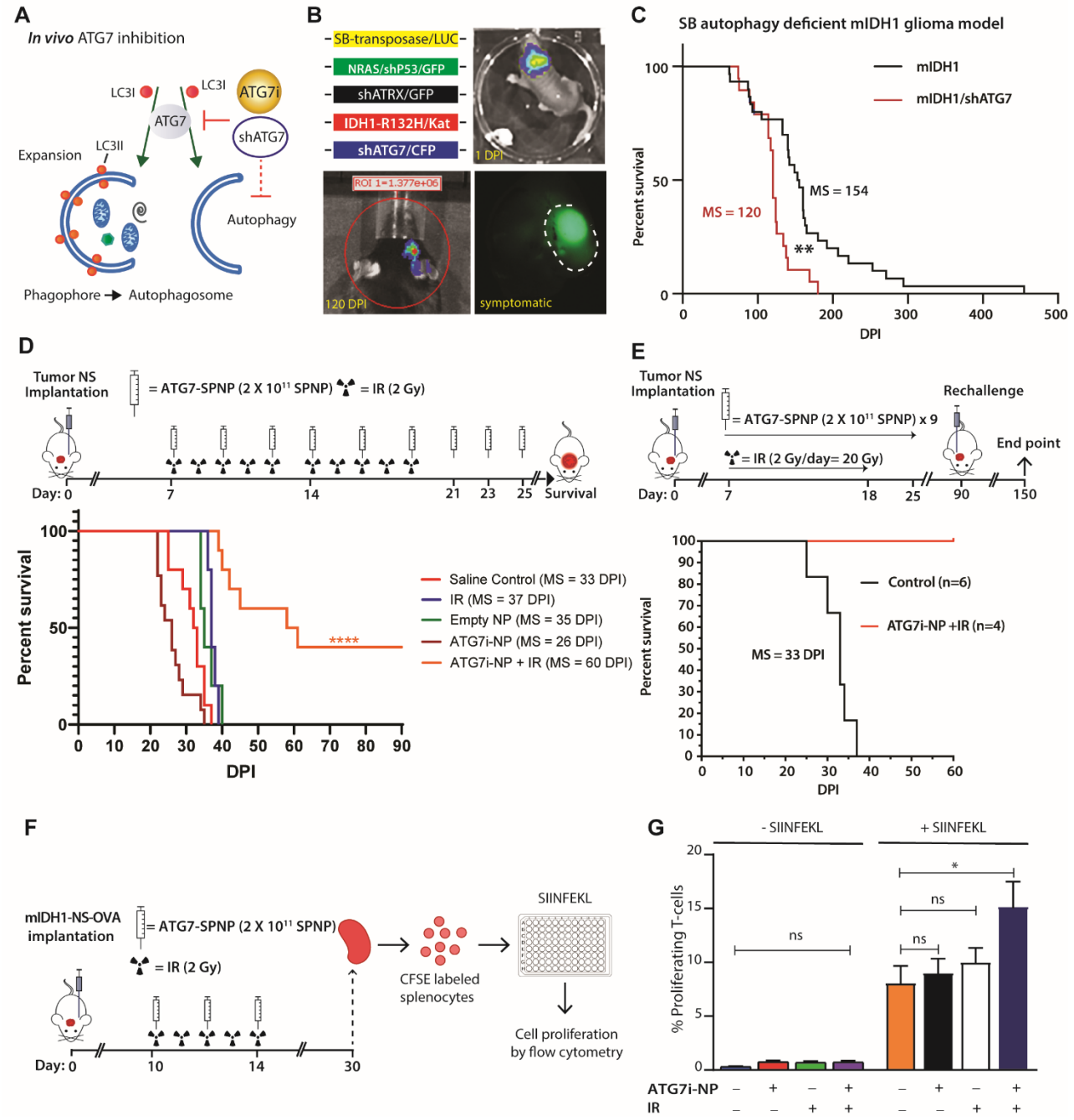

1

Fig. 8. *In vivo* inhibition of autophagy radiosensitizes mIDH1 gliomas and enhances survival. (**A)** SB plasmid encoding shRNA targeting Atg7 (shAtg7) and iRGD SPNPs delivering siRNA (Atg7i) developed for Atg7 inhibition *in vivo*. (**B)** Autophagy deficient mIDH1 mouse gliomas generated using SB transposon system with plasmids encoding SB-transposase-LUC, NRAS/shP53/GFP, shATRX-GFP, $IDH1^{R132H}$/Katushka, and shAtg7/CFP. Transfection efficiency monitored by luminescence. Symptomatic mice brain tumors expressing fluorescent proteins identified macroscopically. (**C)** Kaplan-Meier survival analysis for mice bearing mIDH1 (n=30) or mIDH1 + shATG7 (n=19) gliomas (****P<0.0001, Mantel-Cox test). MS=median survival. (**D)** Autophagy inhibition effect using Atg7i-NP on radio-response in mIDH1 glioma model. Adult mice implanted with 50,000 mIDH1-NS (Day 0). At 7 DPI, animals split into groups: (i) untreated saline control; (ii) 9 doses of $2x10^{11}$ empty SPNPs every other day; (iii) 2 Gy/day; (iv) 9 doses of $2x10^{11}$ Atg7i-NP every other day; (v) 9 doses of $2x10^{11}$ Atg7i-NP every other day and 2 Gy/day (days 7-16). Kaplan-Meier survival analysis performed for each experimental group (***P<0.001, Mantel-Cox test). **(E)** Survival of rechallenged mIDH1 bearing mice, which survived after Atg7i + IR combined treatment. **(F)** Experimental design analyzing Atg7i-NP treatment + IR on T cell proliferation. Mice implanted with 50,000 NPAI-OVA-NS. At 10 DPI, mice treated with 2 Gy/day radiation and Atg7i-NP every other day. Splenocytes collected after 30 DPI. SIINFEKL (100 nM) added to splenocytes. **(G)** T cell proliferation measured as CFSE staining reduction in CD45+/CD3+/CD8+ populations. Bars (mean ± SEM) represent proliferating $CD8^+$ T cell percentage within treatment groups (n=5 replicates; one-way ANOVA followed by Tukey's test. *P<0.01; ns=non-statistically significant).

Graphical Abstract

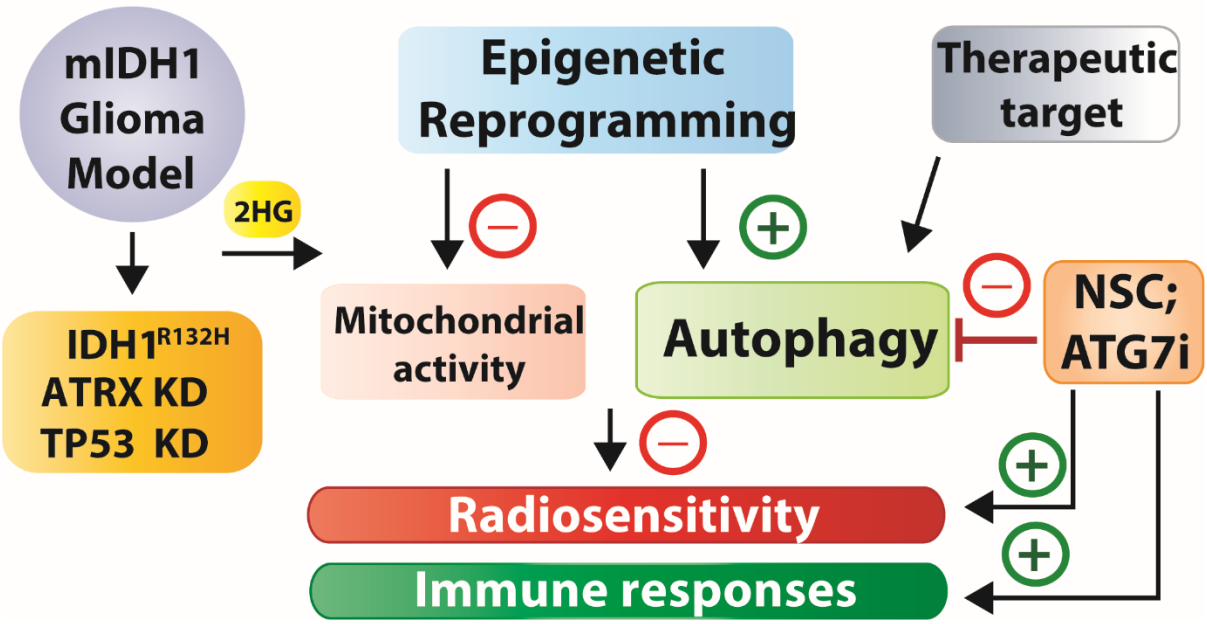

1

Graphical abstract. Our genetically engineered mIDH1 mouse glioma model harbors IDH1^{R132H} in the context of ATRX and TP53 knockdown. The production of 2-HG elicited an epigenetic reprogramming associated with a disruption in mitochondrial activity and an enhancement of autophagy in mIDH1 glioma cells. Autophagy is a mechanism involved in cell homeostasis related with cell survival under energetic stress and DNA damage protection. Autophagy has been associated with radio resistance. The inhibition of autophagy thus radio sensitizes mIDH1 glioma cells and enhances survival of mIDH1 glioma-bearing mice, representing a novel therapeutic target for this glioma subtype with potential applicability in combined clinical strategies.